

Elsevier required licence: © <2022>. This manuscript version is made available under the CC-BY-NC-ND 4.0 license <http://creativecommons.org/licenses/by-nc-nd/4.0/>
The definitive publisher version is available online at [10.1016/j.cherd.2022.07.022](https://doi.org/10.1016/j.cherd.2022.07.022)

Arsenic removal by a pomelo peel biochar coated with iron

Thi Hai Nguyen¹, Paripurnanda Loganathan¹, Tien Vinh Nguyen^{1*}, Saravanamuthu Vigneswaran^{1*}, Thi Hoang Ha Nguyen², Hai Nguyen Tran³, Quoc Bien Nguyen⁴

¹ Faculty of Engineering and IT, University of Technology Sydney (UTS), Sydney, Australia

² University of Science, Vietnam National University, Hanoi, Vietnam

³ Institute of Fundamental and Applied Sciences, Duy Tan University, Ho Chi Minh, Vietnam

⁴ Department of Civil and Environmental Engineering, Pusan National University, Busan, Republic of Korea

* Corresponding authors: Tien Vinh Nguyen, Email: Tien.Nguyen@uts.edu.au; Tel: 61-2-95142620; Fax: 61-2-95147803; Saravanamuthu Vigneswaran Email: Saravanamuth.Vigneswaran@uts.edu.au; Tel. +612- 9514-2641; Fax: +612- 9514-2633.

Abstract

Arsenic pollution is a serious concern in drinking water due to its high toxicity. In this study, pomelo peel biochar coated with iron (PPCI) through slow pyrolysis carbonization and iron-coating processes was investigated for its ability to remove arsenite (As(III)) and arsenate (As(V)). The maximum adsorption capacity of As(III) and As(V) on PPCI at pH = 7 determined by the Langmuir model were 11.77 mg/g and 15.28 mg/g, respectively. The PPCI's adsorption capacity is much higher than that of raw pomelo peel (PP) (0.033 mg/g and 0.034 mg/g for As(III) and As(V), respectively) and many other biomass-derived adsorbents reported in the literature. pH within the 2.0–10 range did not significantly affect PPCI's capacity to adsorb both As ions. In contrast, the presence of co-existing anions caused differential reductions in As removal efficiency ($\text{Cl}^- < \text{SO}_4^{2-} < \text{CO}_3^{2-} < \text{SiO}_3^{2-} < \text{HPO}_4^{2-}$). The characterization of PPCI (morphological, textural, surface functionality, and surface charge properties) before and after

adsorption was conducted. Results show that the adsorption mechanisms were inner-sphere complexation (ligand exchange, hydrogen bonding) and outer-sphere complexation (electrostatic attraction). Demonstrated here is that PPCI is an environmentally friendly material, simple to synthesize from abundant locally available pomelo waste products and has a high potential to efficiently and easily remove the two forms of toxic As anions from water.

Keywords: Arsenic removal; adsorption; iron impregnated biochar; pomelo peel; water treatment

1. Introduction

Arsenic (As) is a highly toxic element derived from both natural environmental processes and human activities ([Smedley and Kinniburgh, 2002](#); [Smith et al., 2016](#)). The presence of excessive levels of As in groundwater in many areas can endanger the health of humans and other living organisms when they use this water for drinking ([Tseng et al., 2000](#)). The safe concentration limit of As in drinking water is as low as 10 µg/L as recommended by the World Health Organization ([Water and Organization, 2004](#)). The health of millions of people in many countries such as Bangladesh, China, India, Cambodia, and Vietnam is at risk due to consuming As contaminated water ([Kim et al., 2011](#); [Smedley and Kinniburgh, 2002](#)). In natural water bodies, inorganic arsenite (As(III)) and arsenate (As(V)) are the predominant chemical species ([Choong et al., 2007](#); [Smedley and Kinniburgh, 2002](#)). As(III) is more poisonous and mobile than As(V) ([Choong et al., 2007](#)). Moreover, As(III) is more difficultly removed from water than As(V) because As(III) exists in an uncharged form (H_3AsO_3) in natural waters ([Smedley and Kinniburgh, 2002](#)). The negatively charged species of As(III) including $H_2AsO_3^-$, $HAsO_3^{2-}$, and AsO_3^{3-} are often largely found at pH_{solution} higher than 9.2 (pK_{a1} 9.2, pK_{a2} 12.1, and pK_{a3} 12.7), while As(V) species often exist as the following anionic forms: $H_2AsO_4^-$, $HAsO_4^{2-}$, and AsO_4^{3-} at pH_{solution} in the range of 3.0–6.0, 7.0–11, and 12–14, respectively (pK_{a1} 2.3, pK_{a2} 6.8, and pK_{a3} 11.5) ([Smedley and Kinniburgh, 2002](#)).

Consequently, due to electrostatic attraction mechanism, the removal of As(V) in water environment by most removal technologies (adsorption, coagulation-flocculation, ion exchange) is more effective than that of As(III) ([Litter et al., 2019](#); [Mohan and Pittman Jr, 2007](#); [Weerasundara et al., 2021](#)).

Among the commonly applied treatment technologies used for As removal from water, adsorption is recognized as the most promising method, especially in decentralized water treatment contexts due to its high removal efficiency, cost-effectiveness, and environmental friendliness ([Hao et al., 2018](#)). A significant number of adsorbents have been used for As removal such as, natural adsorbents (laterite, zeolite, clay minerals) ([Nguyen et al., 2020a](#)); industrial by-products (red mud, iron mine waste sludge) ([Nguyen et al., 2009](#); [Yang et al., 2014](#)); agricultural by-products (biomass-derived adsorbents, biochar, activated carbon) ([Ahmad et al., 2022](#); [Nguyen et al., 2020c](#); [Nham et al., 2019](#)); and synthetic materials (layered double hydroxides nanomaterials, iron-oxide coated materials) ([Nguyen et al., 2021](#)). However, due to practical reasons, new adsorbents based on local and low-cost materials are still required. Compounds containing iron have been shown to be effective in removing As from drinking water ([Aredes et al., 2013](#); [Lakshmipathiraj et al., 2006](#); [Matis et al., 1997](#); [Pierce and Moore, 1982](#)). Iron-based adsorbents can also be magnetically separated after the adsorption process, thereby minimizing secondary pollution and recycling exhausted adsorbents ([Zhang et al., 2013](#)). However, one of the main weaknesses of these adsorbents is linked to their chemical and physical form in which they occur. For example, amorphous hydrous iron oxide (FeOOH) often exists in the form of fine powders or gel. Therefore, it is challenging for it to be completely removed from the treated solution after its use ([Li et al., 2009](#)). Another example is γ -Fe₂O₃ particles, with specific magnetic properties, which may easily form aggregates, thereby rapidly reducing their adsorption efficiency ([Zhang et al., 2013](#)). In general, iron and iron oxide particles are often not easily handled, which limits their practical applicability. This led to rising interest in combining iron with low-cost supporting media to remove As, including man-made

materials such as: cement ([Kundu and Gupta, 2006](#)); sand ([Chang et al., 2008](#); [Herbel and Fendorf, 2006](#)); activated carbon ([Chang et al., 2010](#)); activated alumina ([Kuriakose et al., 2004](#)); peat sorbent ([Kasiuliene et al., 2018](#)); slag ([Zhang and Itoh, 2005](#)); naturally-derived materials like cork granulates ([Pintor et al., 2018](#)); sugarcane bagasse ([Pehlivan et al., 2013](#)); rice husk ([Cope et al., 2014](#); [Pehlivan et al., 2013](#)); seaweeds ([Vieira et al., 2017](#)); or zeolite ([Jeon et al., 2009](#)). The results from these studies demonstrated the high effectiveness of iron-impregnated adsorbents to remove As.

Biochar can provide an excellent matrix to load iron due to its enormous surface area and high porosity ([He et al., 2018](#); [Li et al., 2016a](#)). Other studies show that biochar in combination with oxides/hydroxides functional groups could effectively remove As in aqueous solution through chemical adsorption ([Aredes et al., 2013](#); [Zhang et al., 2013](#)). The utilization of biochar derived from agricultural residues could serve as a practical option for groundwater treatment in developing countries due to its abundant local availability, low-cost, simple preparation, and environmental friendliness.

Pomelo (*Citrus maxima* or *Citrus grandis*) is the largest citrus fruit abundantly available in tropical countries, including Vietnam. With its high biomass, pomelo peel (30% by weight of the fruit, ([Tocmo et al., 2020](#))) can cause environmental pollution when disposed of as waste ([Liang et al., 2014](#); [Wu et al., 2017](#)). Pomelo peel is a promising biomass-derived adsorbent because of its high content of polysaccharides, including cellulose, pectin, and lignin, which provide many functional groups ([Tocmo et al., 2020](#); [Zhang et al., 2019](#)). Pomelo peels have been reported to have effectively removed lead ([Lim et al., 2019](#)), cadmium ([Saikaew et al., 2009](#)), copper ([Tasaso, 2014](#)), and dyes by adsorption ([Jayarajan et al., 2011](#); [Zhang et al., 2019](#)). However, their adsorption efficiency towards anionic species such as arsenate is expected to be poor because they possess negative surface charges which do not favour the adsorption of similarly charged anionic species.

According to [Cheng et al. \(2020\)](#), activated biochar adsorbent produced from pomelo peel provided a high specific surface area (up to 2457 m²/g) and total pore volume (1.14 cm³/g), which were responsible for the large adsorption capacity of tetracycline antibiotic. The large surface area and pore volume as well as the presence of organic functional groups in the biochar can also help to adsorb iron compounds. [Li et al. \(2016b\)](#) successfully coated Fe₃O₄ on the porous surface of biochar derived from spongy pomelo pericarp. In other studies, iron oxide particles coated biochar obtained from the pomelo peel were successfully prepared and used for removing organic compounds such as Reactive Red 21 ([Nguyen et al., 2020d](#)), chrome, phenol ([Dong et al., 2021](#)), and rhodamine B ([Liu et al., 2019](#)). Results of these studies indicate the huge potential of using pomelo peel-derived biochar as an iron-coating adsorbent. However, to the best of our knowledge, no study has yet been published on using this adsorbent to remove As or any other inorganic anionic pollutants from water. The novelties of the study presented in this paper are that a locally available agricultural waste (pomelo peel) was used to prepare an activated biochar of very high surface area and iron with high adsorption capacity to As was successfully impregnated onto this biochar. For the first time such an adsorbent was used to remove an inorganic As pollutant and its mechanisms of removal was studied. The results of this study are also expected to provide valuable information for possibly using this adsorbent in removing other inorganic anionic pollutants in water. The practicality of the study is that pomelo peel is a huge agricultural waste in Vietnam, where serious As problem exists. Therefore, use of this locally available waste to ameliorate the As pollution is very cost effective and an easily acceptable technology by the local people.

In this research, pomelo peel biochar coated with iron (PPCI) was synthesized via the slow pyrolysis carbonization process and then impregnated with iron. Detailed batch tests were conducted to evaluate the PPCI's adsorption performance towards both As(III) and As(V) ions. The adsorption mechanisms were explored using morphological, textural, surface functionality, and surface charge characteristics of PPCI before and after adsorption.

2. Materials and methods

2.1. Chemicals

Iron chloride hexahydrate ($\text{FeCl}_3 \cdot 6\text{H}_2\text{O}$) was purchased from GHTech (Guangdong Guanghua Sci-Tech Co. Ltd). Stock As(III) or As(V) solutions of 1000 mg/L were obtained by dissolving 1730 mg of sodium arsenite (NaAsO_2 , from ACE Chemical Co.) or 4160 mg of sodium arsenate heptahydrate ($\text{Na}_2\text{HAsO}_4 \cdot 7\text{H}_2\text{O}$, from BDH Chemical Ltd.) in 1 L distilled water, respectively. Feed solutions of As(III) or As(V) at different concentrations (from 0.05 to 20 mg/L) were prepared by diluting the As(III) or As(V) stock solutions with distilled water. All chemicals used in this study were analytical grade.

2.2. Preparation of adsorbents

2.2.1 Original pomelo peels

Raw pomelo peels (PP) were collected from fresh pomelo fruits in a supermarket in Hanoi, Vietnam, and subsequently washed three times with tap water, followed by three times with deionized water to remove any impurities. The raw PP was then cut into small pieces (2.5–5 mm) and placed inside an oven at 70 °C for 48 h. The dried PP was finally crushed and sieved into particle sizes varying from 0.25 to 0.5 mm. They were then placed in sealed plastic bags before being employed in subsequent experiments.

2.2.2. Pomelo peels biochar production

In this study, biochar productions from PP at different pyrolysis temperatures (350, 550, and 650 °C) were developed to determine the optimum temperature of production. Briefly, 100 g dried PP of size 0.25–0.5 mm was subjected to slow pyrolysis carbonization for 3 h in an oxygen-free muffle furnace at 350, 550, or 650 °C, respectively. Following the pyrolysis process, the PP biochar formed in the heating process was washed several times with deionized water and then placed inside an oven at 70 °C for 48 h. The resultant biochar productions at

350, 550, and 650 °C of pyrolysis were labelled as PPC-350, PPC-550, and PPC-650, respectively.

A scanning test was conducted to compare the removal efficiency of PP raw and its biochar samples (developed at three different pyrolysis temperatures of 350, 550, and 600 °C) with As(V) solution. The experiment was implemented with 1 g/L of adsorbent dose, 24 h, pH = 7.0, temperature 30 °C, and initial As(V) concentration of 0.4 mg/L. The results (presented in more detail in **Section 3.1**) indicated that the removal efficiency of PPC-350 for As(V) in solution were 12.43%, which was not much different with that of PPC-500 (12.50%) and PPC-600 (14.30%). In fact, increasing pyrolysis temperature increased the energy consumption. Although PPC-350 exhibited a slightly lower adsorption capacity than that of PPC-550 and PPC-650, PPC-350 samples were selected for the subsequent iron coating process due to its low energy consumption and its environmental friendliness.

2.2.3. Pomelo peel's modification with iron

In this study, the biochar produced at 350 °C (PPC-350) was selected for its modification with iron. A PPC-350 sample was firstly dried inside the oven then coated with iron according to the method described by [Nguyen et al. \(2020c\)](#). The procedure used was as follows: 50 g of PPC-350 was soaked into a 150 mL solution of 0.1 M FeCl₃.6H₂O. The pH of the resulting suspension was set at approximately 7.0 by dropwise addition of 2 M NaOH solution. The mixture was then agitated at 160 rpm for 48 h at 30 °C. The solids were separated from the suspension and dried at 70 °C for 48 h. Then the dried solids were rinsed with deionized water several times until the brown colour was removed. All residual fibrous material was dried further at 70 °C for 24 h. To enhance the level of iron grafting, the grafting process was repeated three times. The final iron-modified PPC-350 adsorbents after coating once, twice, and thrice with iron were labelled PPCI-1, PPCI-2, and PPCI-3 and stored in airtight containers. The preparation procedure for the adsorbents is illustrated in **Fig. 1**.

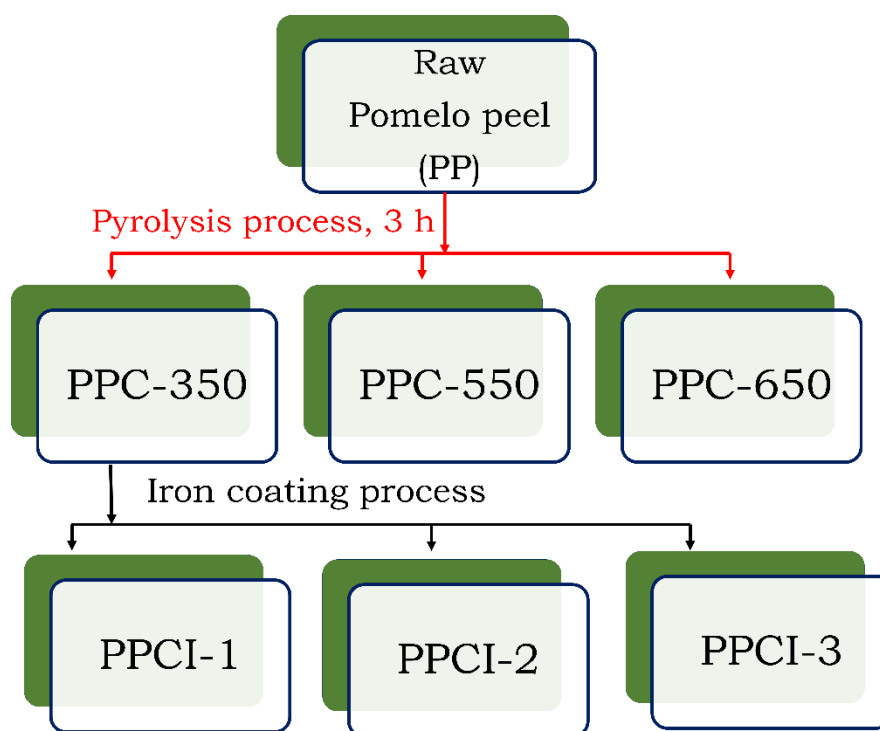


Fig. 1. Schematic illustration of the preparation procedure of the adsorbents

2.3. Batch adsorption experiment

An initial adsorption test was conducted to identify the removal capacity of PP and its modified forms of adsorbents for removing As from synthetic water. The experimental conditions were similar to the scanning test described in **Section 2.2.2**. Approximately 0.1 g of adsorbent was added to 100 mL of As(V) solution in an Erlenmeyer flask. The initial As concentration was fixed at 0.4 mg/L. The flasks were sealed, and then placed on a mechanical shaker, and shaken at 160 rpm for 24 h at 30 °C. After the completion of the experiment, the samples were filtered through a 0.45 µm filter to analyse As(V) concentration in solution.

The equilibrium adsorption study was carried out by mixing either 0.5 g PP or 0.05 g PPCI with 50 mL of As(III) or As(V) solutions. The 100 mL flasks containing the mixed solutions were shaken for 24 h at 30 °C. The initial concentrations of As(III) and As(V) varied from 0.05 to 20 mg/L. Because the As contaminated natural surface and groundwater normally exist at neutral pH, the solution pH in the experiment was kept constant throughout the

experiment at 7.0 ± 0.2 by monitoring the pH solution after 2–3 h and adjusting it to the initial value (pH ~ 7) by adding 0.1 M HNO₃ or 0.1 M NaOH.

The adsorption kinetics experiment was done by mixing 0.05 g PPCI with 50 mL of As(III) or As(V) solutions at initial concentrations of 0.5 mg/L and 1 mg/L, respectively. Samples were taken at 1, 10, 30, 60, 120, 240, 360, 480, 1200, and 1440 min intervals.

The influence of solution pH on As adsorption performance of PPCI was evaluated by changing the pH of the feed solution from 2.0 to 10.0. The adsorbent dosage was 1 g/L and the initial As(III) or As(V) concentration was 0.5 mg/L. The experimental procedure was similar to that used for the equilibrium adsorption experiment. The pHs of the experimental solutions were determined at the end of the experiment.

Sodium salts of five anions, including chloride (Cl⁻), carbonate (CO₃²⁻), monohydrogen phosphate (HPO₄²⁻), sulphate (SO₄²⁻), and silicate (SiO₃²⁻) at concentrations of 10 mM and 100 mM were used to evaluate the effect of coexisting anions on As adsorption capacity of PPCI. As was added to all the solutions to create a concentration of 0.5 mg As/L. The solutions' pH and temperature were kept at 7.0 and 30 °C, respectively.

In all experiments, the ratio of PPCI weight to As solution volume was 1 g to 1.0 L. At pre-determined times, samples of suspensions were withdrawn from the flask and immediately filtered through 0.45 µm filters to separate the solid and liquid components. The solid component was dried at 80 °C for 12 h and then examined for As-laden adsorbent features. The total As concentration in the liquid component (filtrate) was measured by Inductively coupled plasma mass spectrometry (ICPMS-NexION 2000, US). All tests were duplicated, and the mean data were displayed.

The amount of As adsorbed onto PP and PPCI at equilibrium, q_e (mg/g) was calculated using the following **Equation (1)**.

$$q_e = \frac{C_o - C_e}{m_1} V_1 \quad (1)$$

where: C_0 represents the total As concentration (mg/L) at the beginning of the experiment; C_e , stands for the As concentration (mg/L) at equilibrium; m_1 (g) is the adsorbent dosage; and V_1 (L) represents the volume of As solution.

2.4. Characterization of adsorbents

The surface morphology and superficial main elements of PP and PPCI before and after adsorption were determined by Scanning electron microscope (SEM, Quanta-65) and Energy dispersive spectroscopy (EDS), respectively. Their main surface functional groups were identified by Fourier transform infrared spectroscopy (FTIR; Nicolet iS5) using their spectra in the 400 to 4000 cm^{-1} range. Their textural properties were analysed based on the physisorption isotherm of nitrogen at 77 °K (using NOVA touch 4LX). Furthermore, the surface charge characteristics of adsorbents before and after adsorption were determined using the point of zero charge (pH at which the net surface charge is zero, pH_{PZC}) via the pH drift method. The procedure of this method has been reported in our previous study ([Nguyen et al., 2020a](#)).

3. Results and discussions

3.1. Comparison of As(V) adsorption capacity of pomelo peel and its modifications

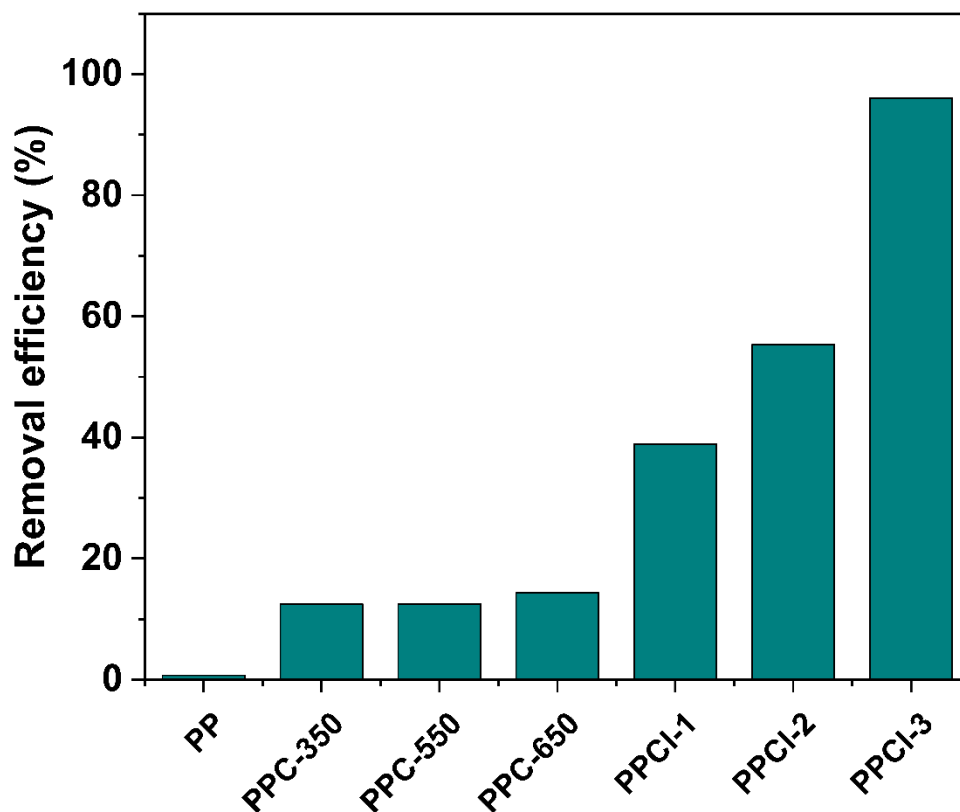


Fig.2. Removal efficiency of As(V) by PP and its modifications

The removal efficiency of As(V) by PP and its modifications is shown in **Fig.2**. Results show that removal efficiency of PP and its different modified adsorbents decreased in the order: PPCI-3 > PPCI-2 > PPCI-1 > PPC-650 > PPC-550 > PPC-350 > PP. Three PP's modification with iron adsorbents (PPCI-1, PPCI-2, PPCI-3) exhibited a remarkably higher adsorption capacity than that of PP and its biochar productions without iron (PPC-350, PPC-550, PPC-650). Additionally, the As(V) adsorption capacity of PP's modification with iron increased with the number of coatings. The removal efficiency of PPCI-3 for As(V) adsorption was 96.02% which is much higher compared to PPCI-2 (55.31%) and PPCI-1 (38.87%). A greater amount

of Fe on the surface of adsorbent produced by three coating times had the highest removal capacity towards As(V). This trend is in line with that reported by [Nguyen et al. \(2020c\)](#). Thus, PPCI-3 was used in the subsequent experiments and with an alternative name as PPCI for more convenience.

3.2. Equilibrium adsorption isotherm

The isotherms for As(V) and As(III) adsorption by PP and PPCI are shown in [Fig. 3](#). The isotherm shapes of PPCI adsorbent are categorized as being L-shaped, suggesting that PPCI's surface has a strong affinity towards As(V) and As(III) ions at small concentrations, which then diminished as concentration increased. The adsorption isotherm models applied in this study were the Langmuir model ([Equation 2](#)) ([Langmuir, 1918](#)), Freundlich model ([Equation 3](#)) ([Freundlich, 1907](#)), Redlich–Peterson model ([Equation 4](#)) ([Redlich and Peterson, 1959](#)). The non-linear forms of these models are described in the following equations.

$$q_e = \frac{Q_{\max}^o K_L C_e}{1 + K_L C_e} \quad (2)$$

$$q_e = K_F C_e^{n_F} \quad (3)$$

$$q_e = \frac{K_{RP} C_e}{1 + a_{RP} C_e^g} \quad (4)$$

where Q_{\max}^o (mg/g) is the Langmuir maximum saturated monolayer adsorption capacity of adsorbent; K_L (L/mg) is the Langmuir constant, which is proportional to the affinity of As to the adsorbent; K_F ((mg/g)(L/mg)ⁿ) is the Freundlich constant related to the strength of adsorption; n_F (dimensionless; 0 < n_F < 1) is a Freundlich intensity parameter; K_{RP} (L/g)

and a_{RP} (L/mg)^g are the Redlich–Peterson constants; and g (dimensionless) is an exponential parameter whose value must be between 0 and 1.

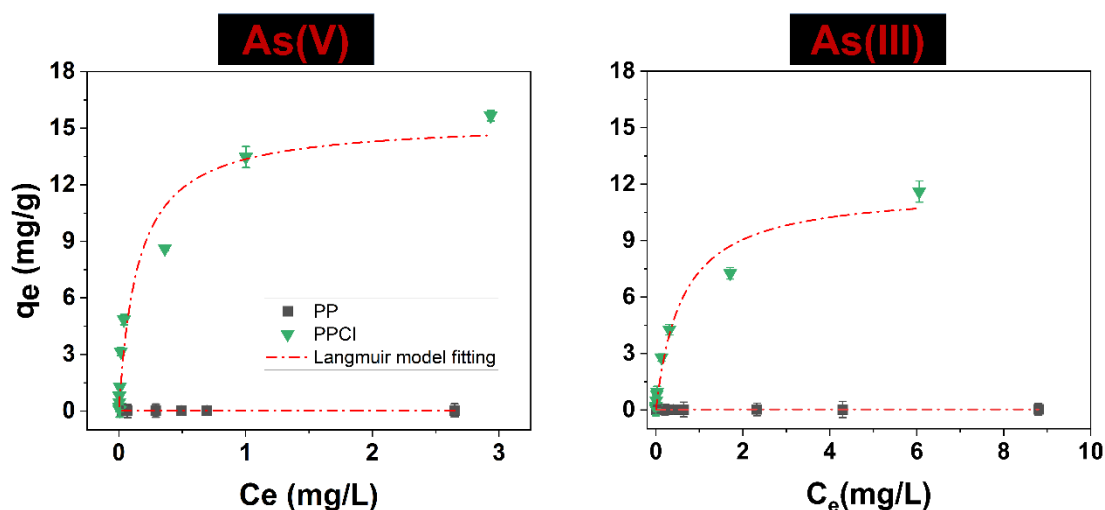


Fig.3. Adsorption isotherms for As(V) and As(III) removal by PP and PPCI (experimental conditions: C_0 As(V) and As(III) = 0.05–20 mg/L, $m/V = 1$ g/L, $t = 24$ h, $pH = 7 \pm 0.2$, temperature 30 °C)

The high R^2 and low χ^2 values (**Table 1**) indicate that the equilibrium adsorption data for both As(V) and As(III) adsorption on PP and PPCI very satisfactorily fitted to all three adsorption models: Langmuir, Freundlich, and Redlich–Peterson. However, the data fits were slightly better with the Redlich–Peterson model, as demonstrated by the slightly greater coefficient of determination (R^2) values ≥ 0.98 (**Table 1**). As stated in **Table 1**, the maximum Langmuir adsorption capacity (Q_{\max}^0) of modified PPCI towards As(V) and As(III) were 15.28 and 11.77 mg/g, respectively, which were extremely higher than those of the raw PP ($Q_{\max}^0 = 0.034$ mg/g for As(V) and $Q_{\max}^0 = 0.033$ mg/g for As(III)).

The As adsorption performance of PPCI was compared to that of other adsorbents reported in the literature (**Table 2**). The modified PPCI material shows an excellent adsorption performance towards both As ions, as demonstrated by its superior adsorption capacity, compared to other adsorbents, including biomass-derived adsorbents (e.g. Luffa plant fibres

([Nguyen et al., 2020c](#)), iron oxy-hydroxides based biomass-derived adsorbents (e.g. Iron-loaded walnut shell, Fe-modified corn stem, Fe-Luffa plant fibres) ([Duan et al., 2017](#); [Lin et al., 2017](#); [Nguyen et al., 2020c](#)), magnetic biochars ([Cope et al., 2014](#); [Kim et al., 2019](#); [Tian et al., 2011](#)), natural iron and manganese oxides minerals ([Lenoble et al., 2004](#); [Nguyen et al., 2020a](#); [Nguyen et al., 2020b](#)), activated carbon and its iron modified activated carbon adsorbents ([Chang et al., 2010](#); [Kalaruban et al., 2019](#)), and iron coated zeolite adsorbents ([Jiménez-Cedillo et al., 2011](#); [Li et al., 2011](#); [Pizarro et al., 2021](#)).

Table 1. Adsorption isotherm model parameters for As(V) and As(III) removal by PP and PPCI

Adsorption parameters	Unit	PP		PPCI	
		As(V)	As(III)	As(V)	As(III)
1. Langmuir model					
Q°_{\max}	mg/g	0.034	0.033	15.28	11.77
K_L	L/mg	6.07	6.43	6.70	1.67
R^2	—	0.99	0.97	0.95	0.97
χ^2	—	$1.81 \cdot 10^{-6}$	$3.50 \cdot 10^{-6}$	1.60	0.50
2. Freundlich model					
K_F	(mg/g)/(mg/L) ⁿ	0.03	0.0235	10.81	5.72
n_F	—	0.30	0.221	0.37	0.40
R^2	—	0.85	0.830	0.95	0.99
χ^2	—	$2.36 \cdot 10^{-5}$	$2.76 \cdot 10^{-5}$	1.43	0.19
3. Redlich–Peterson model					
K_{RP}	L/g	0.18	0.22	260.33	78.80
a_{RP}	(mg/L) ^{-g}	4.90	6.69	20.70	11.54
g	—	1.00	0.99	0.78	0.70
R^2	—	0.98	0.98	0.98	0.99
χ^2	—	$3.17 \cdot 10^{-6}$	$4.06 \cdot 10^{-6}$	0.64	0.03

Note: R^2 is coefficient of determination and χ^2 is Chi-Square values

1 **Table 2.** Comparison of the Langmuir maximum adsorption capacity (Q°_{\max}) values of As(III) and As(V) for PPCI with values for other adsorbents
 2 reported in literature

Adsorbents	Adsorption condition					Q°_{\max} (mg/g)		Ref.
	m/V (g/L)	pH	T (°C)	t (h)	C_0 (mg/L)	As(V)	As(III)	
PP	1.0	7.0	30	24	0.05–20	0.034	0.033	This study
PPCI	1.0	7.0	30	24	0.05–20	15.28	11.77	This study
Luffa plant fibres	1–5	7	25	24	0.5	0.035		Nguyen et al. (2020c)
Iron-loaded walnut shell	1.0	7.0	30	24	0.1–5	—	1.24	Duan et al. (2017)
Fe-modified corn stem	1	7	—	—	0.2–50	8.25	—	Lin et al. (2017)
Fe-Luffa plant fibres	0.003–0.07	7	25	24	0.5	2.55	—	Nguyen et al. (2020c)
Iron oxide amended rice husk char	0.4	6.9	—	—	0.1–2.5	—	1.46	Cope et al. (2014)
Fe-modified biochar beads	2.4	7.9	—	—	1–30	—	11.29	Kim et al. (2019)
Fe ₃ O ₄ coated wheat straw	10	7	—	—	1–28	4.018	3.898	Tian et al. (2011)
Natural laterite (NLTT)	7.5	7.0	25	24	0.1–25	0.58	0.512	Nguyen et al. (2020a)
VMO	2–14	7	25	24	0.5	0.11	-	
Fe-VMO	0.1–2.0	7	25	24	0.5	2.19	-	Nguyen et al. (2020b)
Mixed magnetite–maghemite nanoparticles	0.4	2	—	—	0.5–4	3.71	3.69	Chowdhury and Yanful (2010)
GACs	0.1–0.8	6.0	25	24	0.1	—	1.01	
GAC-Fe	0.1–0.8	6.0	25	24	0.1	—	1.43	Kalaruban et al. (2019)
Fe-GACs	2.5	6.9	25	48	—	—	1.95	Chang et al. (2010)
Iron–manganese-modified zeolite-rich tuffs	10	6.5	18	24	0.05–2	0.06	0.10	Jiménez-Cedillo et al. (2011)
Fe-exchanged natural zeolite	20	—	—	24	0.1–20	0.10	0.05	Li et al. (2011)

3

1 3.3. Kinetics of adsorption

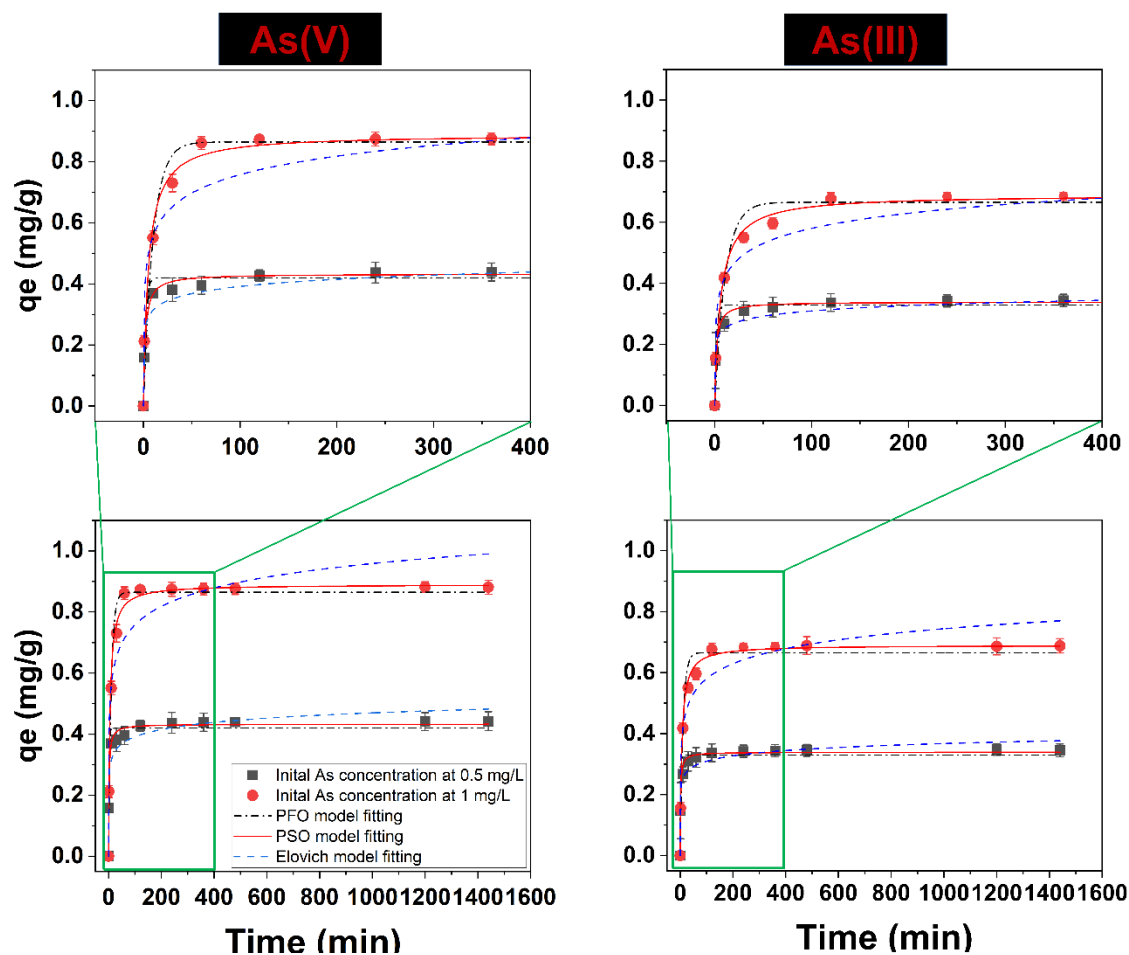
2 **Fig. 4** presents the results of the experiments on the time-dependent adsorption of
3 As(III) and As(V) ions by PPCI at two different initial As concentrations (0.5 mg/L and 1
4 mg/L). The adsorption rate of As(V) and As(III) onto PPCI was very rapid during the first 30
5 min of the experiment. Afterward, the adsorption process continued at a relatively slower rate
6 until it reached a plateau and equilibrium after approximately 120 min. The initial fast
7 adsorption is due to an ample amount of vacant adsorption sites on the PPCI surface at the initial
8 stage, which shrank later on because the adsorption sites were progressively filled up. At a later
9 stage, the remaining vacant surface sites are difficult to occupy due to repulsive forces occurring
10 between the As species on the solid and bulk phases, and therefore the rate of adsorption
11 dropped ([Yao et al., 2014](#)). In this study, pseudo-first-order ([Lagergren, 1898](#)), pseudo-second-
12 order ([Blanchard et al., 1984](#)), and Elovich models ([McLintock, 1967](#)) were employed to
13 describe the intrinsic adsorption constants given in **Equations 5, 6, and 7**, respectively. The
14 nonlinear methods were applied to compute the paramaters of those models.

$$q_t = q_e [1 - \exp(-k_1 t)] \quad (5)$$

$$q_t = \frac{q_e^2 k_2 t}{1 + q_e k_2 t} \quad (6)$$

$$q_t = \frac{1}{\beta} \ln(1 + \alpha \beta t) \quad (7)$$

15 where q_t (mg/g) and q_e (mg/g) are the amount of adsorbate uptake onto adsorbent at any time t
16 and at equilibrium, respectively; k_1 (1/min), k_2 [g/(mg×min)], and α [mg/(g×min)] are the rate
17 constants of the pseudo-first-order model, the pseudo-first-order model, and the initial rate
18 constant of the Elovich models, respectively, β (mg/g) is the desorption constant during any one
19 experiment.



1
2 **Fig. 4.** Kinetics of As(V) and As(III) adsorption onto PPCI (experimental conditions: Co
3 As(V) and As(III) = 0.5 and 1 mg/L, m/V = 1 g/L, pH = 7 ± 0.2)

4
5 The relevant kinetic model parameters for the As adsorption onto PPCI at two initial As
6 concentrations are presented in **Table 3**. The PSO model with a high coefficient of
7 determination value ($R^2 = 0.99$) and low Chi-square value ($\chi^2 = 0.0001-0.001$) described the
8 kinetic adsorption data better than the PFO ($R^2 = 0.96-0.97$ and $\chi^2 = 0.0006-0.0029$) and
9 Elovich ($R^2 = 0.916-0.950$ and $\chi^2 < 0.004$) models. Others have reported that because the PSO
10 model fitted adsorption of As on iron hydroxide/oxides better than PFO model the mechanism
11 of As adsorption is probably chemical, presumably mediated by inner-sphere complexation of
12 the As species with iron hydroxide/oxides ([Hao et al., 2018](#); [Kalaruban et al., 2019](#); [Nguyen et](#)
13 [al., 2020c](#)). This interpretation is consistent with that made from the point of zero charge data
14 discussed later (**Section 3.6.3**) where As adsorption reduced the point of zero charge of PPCI

1 and this was explained as due to chemical adsorption of As. [Kalaruban et al. \(2019\)](#) reported
 2 that the kinetics of As adsorption on granulated AC (GAC) were explained better by PFO, but
 3 when iron was coated on GAC the kinetic data fitted better to PSO. Based on these results, they
 4 reported that the adsorption on GAC was mostly physical whereas that on iron-coated GAC
 5 was chemical.

6

7 **Table 3.** Kinetic model parameters for As(V) and As(III) uptake by PPCI

		Adsorbate			
Unit	As(V)		As(III)		
	Co = 0.5 mg/L	Co = 1 mg/L	Co = 0.5 mg/L	Co = 1 mg/L	
PFO model					
q_e	mg/g	0.420	0.865	0.329	0.665
k_1	1/min	0.444	0.100	0.573	0.093
R^2	—	0.969	0.972	0.955	0.962
χ^2	—	0.0007	0.0029	0.0006	0.0024
PSO model					
q_e	mg/g	0.433	0.890	0.339	0.689
k_2	g/(mg×min)	1.254	0.222	1.864	0.238
R^2	—	0.991	0.990	0.988	0.990
χ^2	—	0.0002	0.0010	0.0001	0.0006
Elovich model					
α	mg/(g×min)	35.083	5.164	57.415	2.420
β	mg/g	29.493	11.465	39.874	14.023
R^2	—	0.931	0.916	0.950	0.938
χ^2	—	0.0016	0.0091	0.0006	0.0040

8

9 As shown in [Table 3](#), there is a remarkable decrease in the PSO adsorption rate
 10 constant (k_2) value when the initial concentrations of As(III) and As(V) increased from 0.5
 11 mg/L to 1 mg/L. At higher initial As concentration, there was greater competition for adsorption

1 than at lower concentrations and this might have reduced the adsorption rate. A similar finding
2 was documented by [Yao et al. \(2014\)](#).

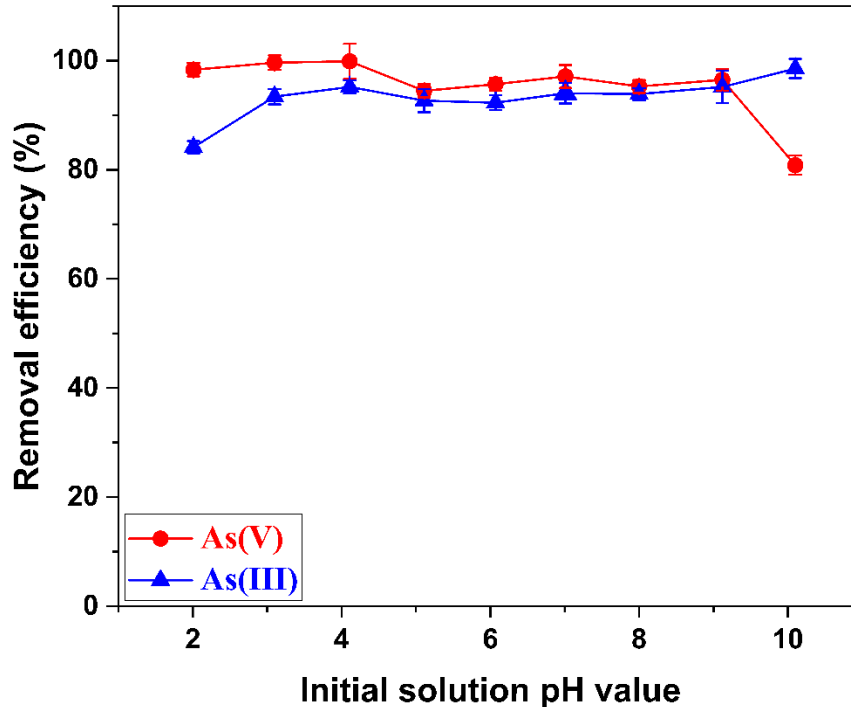
4 **3.4. Influence of solution pH on the adsorption of As ions**

5 The effect of solution pH (2.0–10) on the adsorption of As(III) and As(V) by PPCI is
6 presented in [Fig. 5](#). The capacity of PPCI to adsorb As(III) and As(V) was insignificantly
7 controlled by the pH within the 2.0 to 10 range. The efficiency of PPCI in adsorbing As(V) fell
8 slightly when the pH solution rose from 2.0 to 10. In contrast, there was a minor increase in the
9 adsorption capacity of As(III) by PPCI at low and high pHs.

10 In fact, within the pH solution range from 2 to 10, two anionic forms of As(V) tended
11 to predominate, including monovalent H_2AsO_4^- (pH= 3.0–6.0) and divalent HAsO_4^{2-} (pH =
12 7.0–10) ([Smedley and Kinniburgh, 2002](#)). PPCI possessed a pH_{PZC} of 7.3, suggesting that the
13 PPCI surface was positively charged at solution pH lower than 7.3 (detailed information on
14 pH_{PZC} is presented in [Section 3.6.3](#)). Thus, at pH lower than 7.3, significant amounts of As(V)
15 anions were probably removed by PPCI through electrostatic attraction (outer-sphere
16 complexation). When pH was higher than 7.3, both the adsorbent and adsorbate had negative
17 charges, and therefore the adsorption process is unlikely to occur through electrostatic
18 attraction. Other adsorption mechanisms, namely inner-sphere complexation by ligand
19 exchange ([Hao et al., 2018](#); [Kalaruban et al., 2019](#)), and hydrogen bonding ([Yee et al., 2019](#))
20 might have largely operated in removing As(V) in the solution.

21 In the case of arsenite (As(III)), within the pH range of 1.0 to 9.0, only the uncharged
22 form of As(III) ($\text{H}_3\text{AsO}_3^\circ$) is present ([Mondal et al., 2007](#); [Smedley and Kinniburgh, 2002](#)).
23 Thus, PPCI could not remove the uncharged $\text{H}_3\text{AsO}_3^\circ$ through the electrostatic attraction
24 mechanism. [Fig. 5](#) shows that the removal efficiency of PPCI towards As(III) was slightly lower
25 than that of As(V). However, more than 82% of As(III) was removed. The significant amount
26 of As(III) removal is possibly due to other mechanisms of adsorption, such as hydrogen bonding

1 (between oxygen in As(III) species and hydrogen in hydroxide group in biochar) (Yee et al.,
2 [2019](#)).



3
4 **Fig. 5.** Effect of pH solution on the removal capacity of PPCI towards As(V) and As(III)
5 (experimental conditions: Co As(V) and As(III) = 0.5 mg/L, m/V = 1 g/L, t = 24 h)

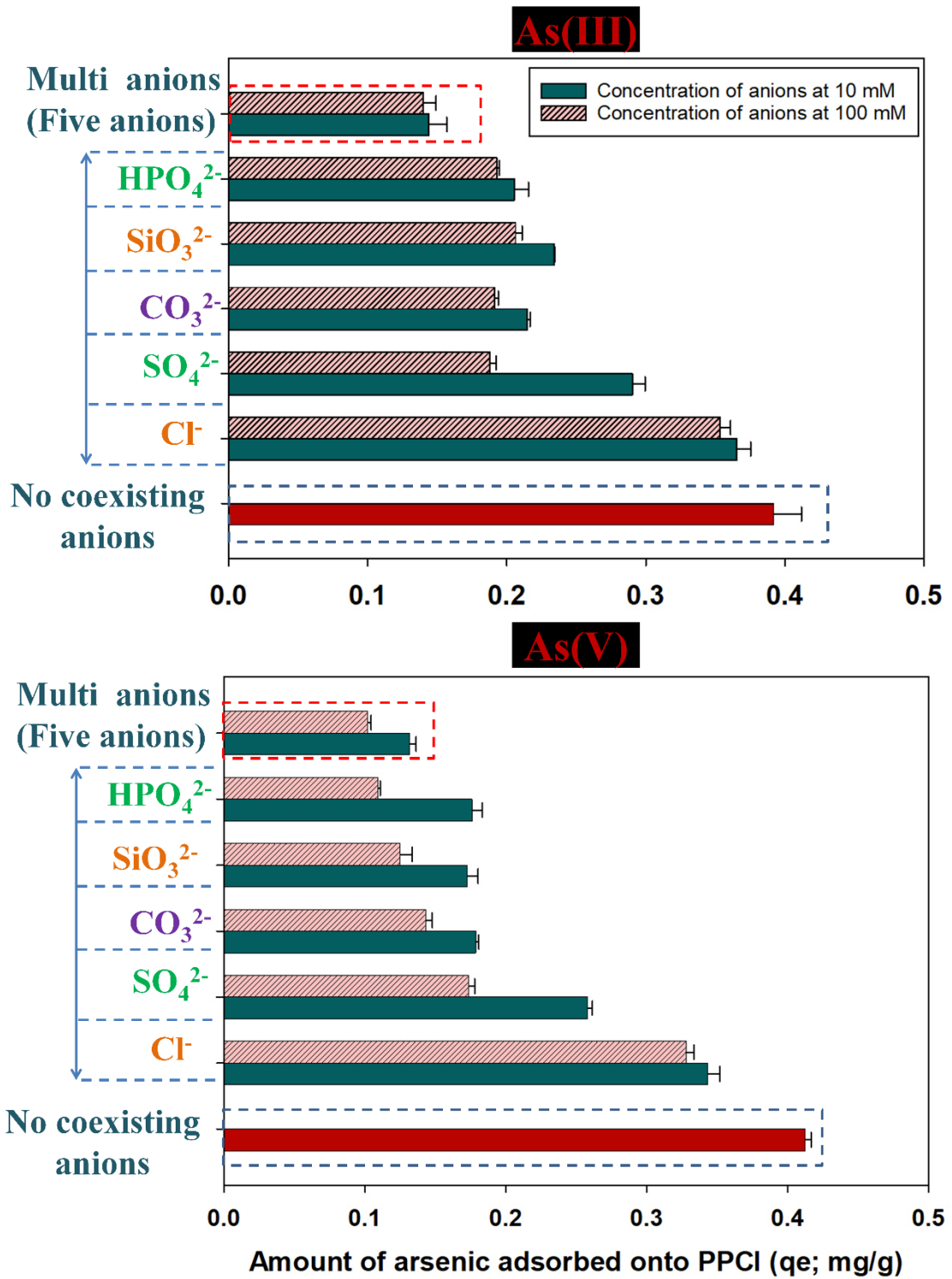
6 7 **3.5. Influence of coexisting single and mixed anions on As(III) and As(V) adsorption**

8 To evaluate the influence of the presence of coexisting anions on As removal of PPCI,
9 five anions (Cl^- , SO_4^{2-} , CO_3^{2-} , SiO_3^{2-} , and HPO_4^{2-}) were tested at two concentrations, these
10 being 10 mM and 100 mM. These anions were mixed with As ions individually or in
11 combination. **Fig. 6** shows that the presence of coexisting anions caused a remarkable
12 reduction in the efficiency of removing As(III) and As(V). The adsorption capacity of PPCI
13 towards both As(III) and As(V) decreased in the order, chloride (Cl^-) > sulphate (SO_4^{2-}) >
14 carbonate (CO_3^{2-}) > silicate (SiO_3^{2-}) > monohydrogen phosphate (HPO_4^{2-}) > the five anions in
15 combination (Cl^- , SO_4^{2-} , CO_3^{2-} , SiO_3^{2-} , and HPO_4^{2-}). As shown in **Fig. 6**, the presence of

1 HPO_4^{2-} had the greatest single anion influence on PPCI's efficiency in removing both As(III)
2 and As(V). The similar tetrahedral structures of As(V) and HPO_4^{2-} and the presence of As and
3 P in the same group in the periodic table (therefore, similar chemical properties) is probably the
4 reason for the strong competition of HPO_4^{2-} with As ions in the adsorption process.

5 These ions have been reported to be chemically adsorbed by inner-sphere complexation
6 usually involving the ligand exchange mechanism (adsorbent surface OH groups exchanging
7 with As and phosphate anions) on Fe-based adsorbents ([Hao et al., 2018](#); [Kalaruban et al., 2019](#);
8 [Loganathan et al., 2014](#); [Nguyen et al., 2020c](#)). In contrast, the As removal efficiency by PPCI
9 adsorbent was insignificantly affected by Cl^- in the solution. This is because Cl^- is monovalent,
10 possesses poorer ionic potential, lacks a tetrahedral structure, and adsorbed on adsorbents by
11 physical processes (outer-sphere complexation/electrostatic forces). These results are
12 consequently consistent with the results of other studies ([Foroutan et al., 2019](#); [Hongtao et al.,](#)
13 [2018](#); [Loganathan et al., 2014](#); [Nguyen et al., 2020a](#); [Yao et al., 2014](#)).

14 The competition of coexisting single and mixed anions with As(V) adsorption was
15 slightly stronger than that with As(III) adsorption. This is partly because As(V) ions are present
16 as anions at pH 7, and this means they compete more with coexisting anions compared to As(III)
17 which is present as uncharged $\text{H}_3\text{AsO}_3^\circ$.



1

2 **Fig. 6.** Influence of coexisting anions (at two initial concentrations of 10 mM and 100 mM)

3 on the adsorption capacity of PPCl towards As(V) and As(III) ions (experimental conditions:

4 Co As(V)/As(III) = 0.05 mg/L, m/V = 1 g/L, t = 24 h, pH = 7 ± 0.2)

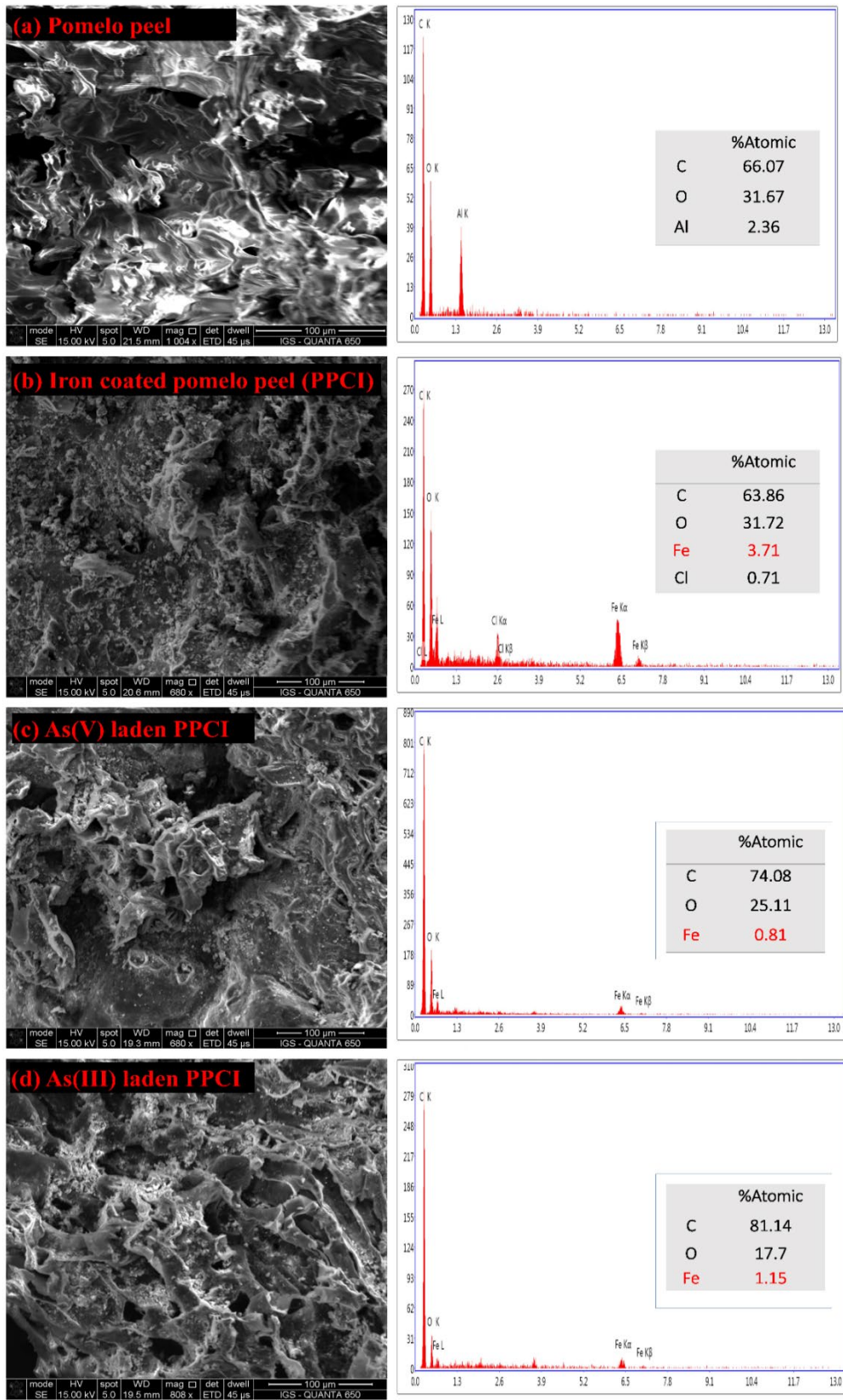
5

1 **3.6. Physico-chemical properties of adsorbent**

2 **3.6.1. Morphology and surface elemental composition (EDS)**

3 The surface morphologies of raw PP and pristine PPCI are presented in **Fig. 7**. The raw
4 PP possessed a highly porous structure with a smooth surface, suggesting that it exhibits a large
5 surface area. Conversely, the modified PPCI possessed a wrinkled, irregular, and heterogeneous
6 surface morphology. The heterogeneous surface is due to the aggregation/agglomeration of iron
7 particles and their extensive uneven distribution on the PPCI surfaces. Most of the micropores
8 and ultra-micropores of PPCI adsorbent were blocked or clogged by iron particles, leading to a
9 shrinkage in surface area and pore volume of PPCI. This explanation is supported by textural
10 properties data presented in the next section (**Section 3.6.2**). The As(III) and As(V)-laden PPCI
11 also possessed a wrinkled, irregular, and heterogeneous surface morphology, which did not
12 differ much from that of PPCI before adsorption (**Fig. 7**).

13 In addition to morphology, element analysis (EDS) of the adsorbent surfaces was
14 conducted (**Fig. 7**). The results indicate that C is a predominant element in both PP and PPCI
15 adsorbents (atomic percentage of 66.07% and 63.86%, respectively), reflecting the composition
16 of pomelo peel biochar. PPCI possessed a small amount of Fe (3.71% in atomic composition,
17 corresponding to 13.75% in total weight), suggesting that the iron was successfully
18 incorporated onto PPCI during its synthesis. The original PP before incorporation of Fe
19 contained no detectable amount of Fe.

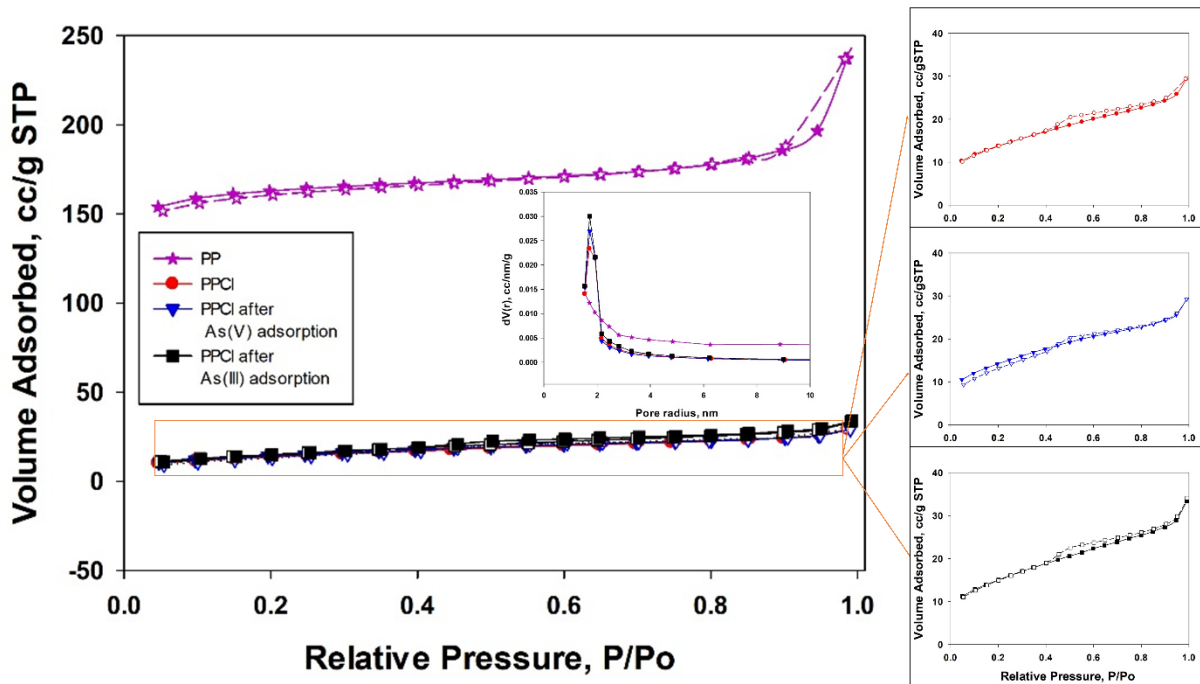


1
 2 **Fig. 7.** SEM-EDS data of (a) raw PP, (b) pristine PPCI, (c) As(V) - laden PPCI, and (d) As(III)
 3 - laden PPCI

4

1 **3.6.2. Texture**

2 The isotherm graphs of N₂ adsorption at 77 °K of PP and PPCI adsorbents are shown in
 3 **Fig. 8**. Based on the IUPAC technical report by [Thommes et al. \(2015\)](#), N₂ adsorption and
 4 desorption isotherms of PP adsorbent are classified as II type with an H3 type hysteresis loop
 5 (relative pressure of p/p₀ > 0.8). These results suggest that PP is a porous adsorbent. The
 6 N₂ adsorption and desorption graph for PPCI samples exhibited two things: a IV type
 7 physisorption isotherm and H3 type hysteresis loop. For this reason, it is expected that the PPCI
 8 adsorbent is mesoporous and this conclusion is consistent with what [Coville and Tshavhungwe](#)
 9 [\(2010\)](#) reported.



10
11

12 **Fig. 8.** Nitrogen adsorption and desorption isotherms of raw PP, pristine PPCI and As-laden
 13 PPCI

14

15 **Table 4** presents the surface area (S_{BET} ; determined from the Brunauer-Emmett-Teller
 16 and total pore volume (V_{total} ; calculated from the BJH) of the adsorbents using the N₂ adsorption
 17 data. PP exhibited a S_{BET} of 48.65 m²/g and a total pore volume of 0.13 cm³/g, which were
 18 remarkably higher than those of PPCI (5.43 m²/g and 0.0289 cm³/g, respectively). A notable

1 reduction in surface areas and pore volume of PPCI was probably due to iron particles and their
 2 aggregates dispersing widely on its surface and closely blocking most of its macropores and
 3 micropores. These results demonstrate that the blockage process or pore filling of iron oxides
 4 inside the carbon matrix leads to remarkably increasing of the iron oxide content in PPCI. Other
 5 researchers also reported that a reduction in surface area and pore volume of adsorbent can
 6 occur after the iron-impregnation process. According to [Kalaruban et al. \(2019\)](#), BET surface
 7 and pore volume of the modified GAC-Fe were 876 m²/g and 0.60 cm³/g, which were much
 8 lower than that of GAC (1124 m²/g and 0.62 cm³/g). The surface area and pore volumes of
 9 As(V) and As(III)-laden adsorbents were not much different from those of PPCP before
 10 adsorption (As(V), 4.72 m²/g and 0.0295 cm³/g, respectively; As(III), 3.20 m²/g and 0.0354
 11 cm³/g, respectively), which implies that the pores are still blocked, this time probably by Fe/As
 12 reaction products formed after adsorption.

13 **Table 4.** Physical properties of adsorbents

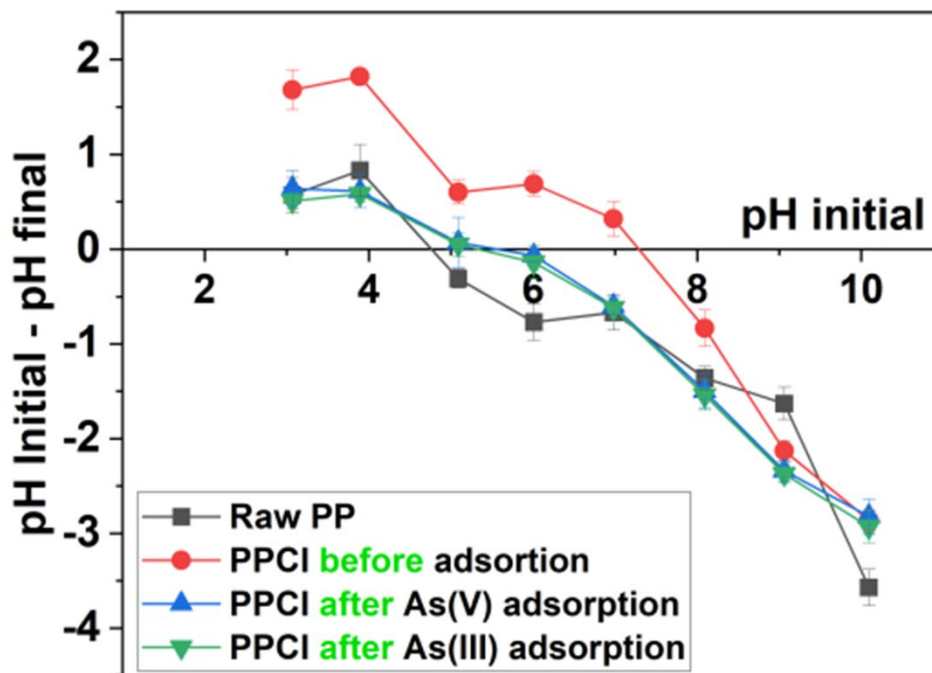
Adsorbents	BET surface area	Pore volume	Pore radius
	m ² /g	cm ³ /g	nm
PP	48.65	0.13	1.53
PPCI	5.43	0.0289	1.709
PPCI after As(V) adsorption	4.72	0.0295	1.726
PPCI after As(III) adsorption	3.20	0.0354	1.721

14

15 **3.6.3. Point of zero charge (pH_{PZC})**

16 The point of zero charge (pH_{PZC}) of raw PP and PPCI before and after As adsorption was
 17 determined by the pH drift method. As shown in [Fig. 9](#), pH_{PZC} of the raw PP material was 4.8.
 18 This result agrees with the pH_{PZC} for other biomass-derived adsorbents such as raw orange peel
 19 (pH_{PZC} = 5.3) ([Tran et al., 2016](#)), and *Nauclea diderrichii* seed (pH_{PZC} = 4.9) ([Omorogie et al.,](#)
 20 [2016](#)). The PPCI had a pH_{PZC} of 7.3, which was significantly higher than that of raw PP. The

1 higher pH_{PZC} of PPCI was caused by the iron-coating process where the impregnation of
 2 positively charged Fe caused increased positive charges on PPCI surface and therefore raised
 3 the pH at which the net surface charge is zero (pH_{PZC}). A similar increase was reported in a
 4 previous study on iron modified rice straw biochar, where the pH_{PZC} of raw rice straw biochar
 5 (BC) increased from 5.44 to 6.88 when Fe was incorporated into BC (Nham et al., 2019). Thus,
 6 the external surface of PPCI exhibited some positive charges in this study where the solution
 7 pH value was maintained at 7. Therefore, PPCI could remove As(V) anions from solution
 8 through electrostatic attraction mechanism.



9
 10 **Fig. 9.** pH_{PZC} values of raw PP ($pH_{PZC} = 4.8$), pristine PPCI ($pH_{PZC} = 7.3$), PPCI after
 11 adsorption of As(V) ($pH_{PZC} = 5.8$), and PPCI after adsorption of As(III) ($pH_{PZC} = 5.4$)
 12

13 The pH_{PZC} values decreased from 7.3 to 5.8 and 5.4 after As(V) and As(III) adsorption,
 14 respectively as shown in **Fig. 9**. This decrease in pH_{PZC} values suggests that both these As ions
 15 have reacted with PPCI by inner-sphere complexation adding negative charges to PPCI surface,

1 thereby decreasing the pH at which the net surface charge became zero (pH_{PZC}). Decreases in
2 pH_{PZC} after As adsorption were also reported for other Fe-based adsorbents ([Faria et al., 2014](#);
3 [Pereira et al., 2019](#)).

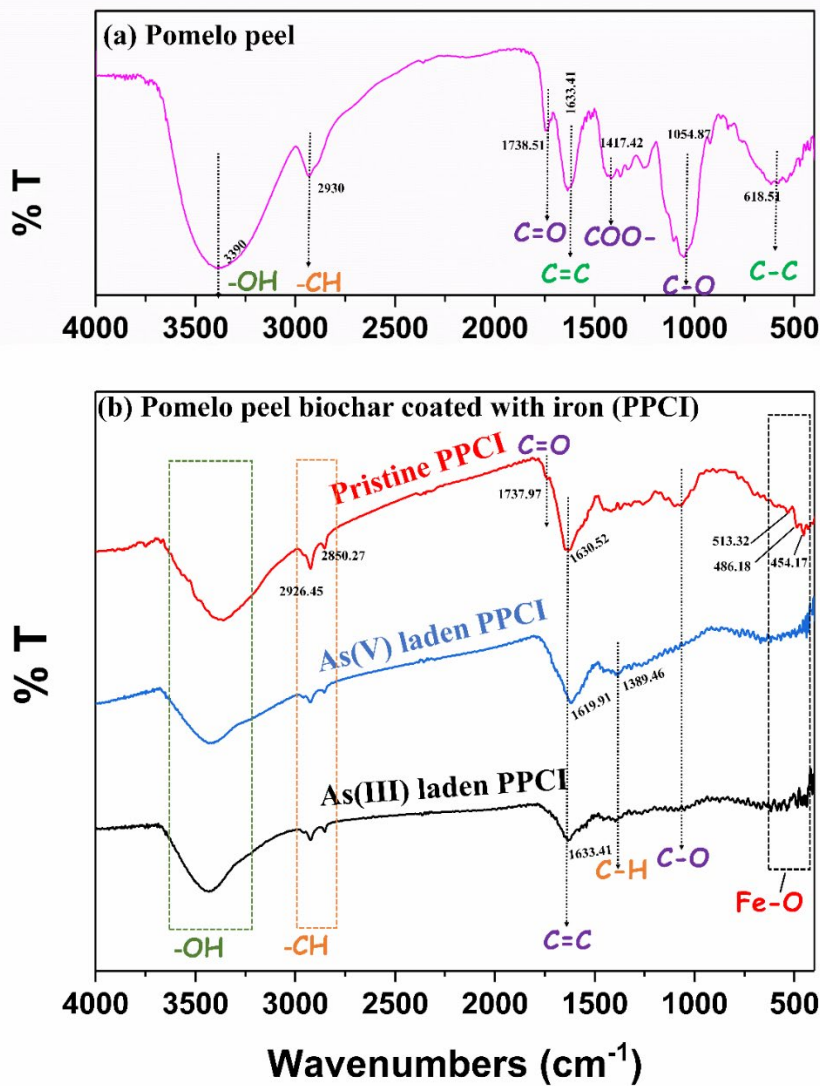
4

5 **3.6.4. Surface functionality**

6 The main functional groups on adsorbents' surface were determined by the FTIR
7 technique (**Fig. 10**). The FTIR spectrum of raw PP (purple solid line) is presented in **Fig.**
8 **10a**. The highlighted broad spectra band located at the peak around of 3390 cm^{-1}
9 (corresponding to the presence of $-\text{OH}$ groups) show the stretching vibrations of $-\text{OH}$ group
10 presented in adsorbed water ([Nguyen et al., 2020a](#); [Oliveira et al., 2009](#)). The narrower peak at
11 approximately 2930 cm^{-1} is attributed to the $-\text{CH}$ stretching bond, which means $-\text{CH}_2$ and $-\text{CH}$
12 groups are present ([Oliveira et al., 2009](#)). Two small spectral bands at 1738 cm^{-1} and 1417
13 cm^{-1} are assigned to the stretching of $\text{C}=\text{O}$ and COO^- , respectively, which were probably from
14 carboxylic acids, esters, and anhydrides. A sharp peak at 1633 cm^{-1} is attributed to $\text{C}=\text{C}$ surface
15 functional groups ([Tomul et al., 2020](#)). The peak for the stretching vibration of $\text{C}-\text{O}$ bonds
16 could be seen at 1054 cm^{-1} . The peaks at around 618 cm^{-1} are ascribed to $\text{C}-\text{C}$ bond ([El-Naggar](#)
17 [et al., 2020](#)).

18 The FTIR spectrum of pristine and As-laden PPCI samples still exhibited several typical
19 functional groups as in PP after the modification and adsorption process (**Fig. 10b**). Some
20 important functional groups on the pristine PPCI and As-laden PPCI's surface were well
21 identified at several corresponding peaks at approximately 1630 cm^{-1} ($\text{C}=\text{C}$) and 1054 cm^{-1}
22 ($\text{C}-\text{O}$). The broad spectra bands in the region between 3800 and 3000 cm^{-1} could be attributed
23 to the $-\text{OH}$ stretching vibration. The $-\text{CH}$ stretching is detected at a broad band of 2800 – 2929
24 cm^{-1} . A peak, although small at 1737 cm^{-1} is attributed to $\text{C}=\text{O}$ bond, which was quite hardly
25 visible on the surface of pristine PPCI adsorbent. Particularly, the broad spectral band at around
26 500 cm^{-1} (including three small peaks at 445.17 , 486.18 , and 513.32 cm^{-1}) was assigned to the

1 Fe–O groups (Baig et al., 2016; Chaudhry et al., 2017), which was well observed on pristine
2 PPCI's surface but not observed in raw PP. This result indicates that the iron grafting process
3 on PPCI adsorbent was successful, and it is also supported by SEM results, as well as elemental
4 analysis data (EDS) (Section 3.6.1). In addition, after As(V)/As(III) adsorption process, Fe–O
5 groups were found to be absent on the surface of As-laden adsorbents, probably because Fe has
6 reacted with As by breaking the Fe–O bond (Fig. 10b).



7
8
9

Fig. 10. FTIR spectrum of (a) raw PP and (b) pristine and As-laden PPCI

3.7. Adsorption mechanisms

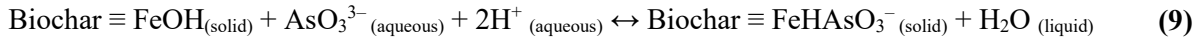
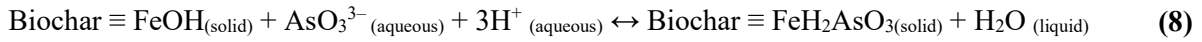
Generally, the possible mechanisms of As adsorption by iron-coated biochar includes a number of interactions. The S_{BET} of PPCI (5.43 m²/g) is remarkably lower than that of typical commercial activated carbon (CAC) (>1000 m²/g) ([Lee et al., 2007](#)), modified activated carbon (388 to 1747 m²/g) ([Arcibar-Orozco et al., 2014](#)). Thus, the contribution of pore filling mechanism in removing As by PPCI from water is not important as other mechanisms, such as electrostatic attraction. The value of pHPZC of PPCI (**Section 3.6.3**) prior to and after adsorption process suggest that electrostatic adsorption (outer-sphere complexation) probably occurred because the pHPZC (pH 7.3) of PPCI was slightly higher than pH of the experimental solution (pH 7). Similar findings were reported elsewhere ([Amen et al., 2020](#); [Dixit and Hering, 2003](#); [Samsuri et al., 2013](#); [Vithanage et al., 2017](#); [Yee et al., 2019](#)).

Hydrogen bonding mechanism is considered as a predominant interaction between As and certain adsorbents. The main common feature of those adsorbents is that they possess abundant oxygen and hydrogen-containing functional groups in their surfaces. In this study, FTIR results also indicate that there was a remarkable number of oxygen and hydrogen-bearing functional groups (C–O, –OH, C=O) in pristine PPCI. These could be responsible for H-bonding with the hydrogen and oxygen atoms in As(III)/As(V) ions in solution. This explanation agrees with what has been intensively reported in several studies ([Khatamian et al., 2017](#); [Verma and Singh, 2019](#); [Vithanage et al., 2017](#)).

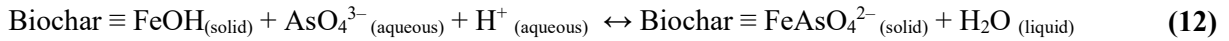
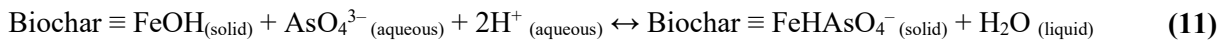
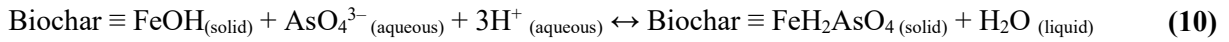
According to [Vithanage et al. \(2017\)](#), the iron-coating on the iron-coated biochar was present in the form of iron oxides largely as magnetite and hematite. Both the reduced form (Fe²⁺) and the oxidized form (Fe³⁺) of iron dominated the iron-coated biochar adsorbents. These iron oxides could oxidize the more toxic As(III) ion into less toxic As(V) ion. The As(III) and oxidized As(V) were then probably chemically adsorbed on iron oxides by the inner-sphere complexation mechanism.

1 The possible inner-sphere complexation mechanisms of As(III) and As(V) adsorption
2 on the iron-coated biochar are described by **Equations 8–12** given below :

3 For As(III) ions:



4 For As(V) ions:



5 The chemical adsorption of As ions by inner-sphere complexation is supported by the
6 reduction in pH_{PZC} observed when these ions were adsorbed (as discussed in **Section 3.6.3**).

7

8 **4. Conclusions**

9 Pomelo peel biochar coated with iron (PPCI) was successfully synthesized via slow
10 pyrolysis and iron grafting processes. PPCI possessed a pH_{PZC} of 7.3, which suggests that its
11 surface contains positive charges at natural water for favourable adsorption of the negatively
12 charged As species. Significant amounts of O– bearing functional groups (C–O, –OH, C=O) in
13 PPCI play a significant role in strong H-bonding and/or surface complexation formation with
14 As(III) and As(V) ions in solution. However, the much higher adsorption capacity (Langmuir
15 adsorption capacity, mg/g) of PPCI (As(III) 11.77, As(V) 15.28) compared to unmodified
16 pomelo peel adsorbent (As(III) 0.33, As(V) 0.34) is largely due to inner-sphere complexation
17 of As species with Fe in PPCI. PPCI had superior adsorption capacity compared to many other
18 biomass-derived adsorbents including those modified with Fe reported in literature. The
19 presence of coexisting anions reduced the adsorption capacity of PPCI, with the effect being

1 strong for other inner-sphere complexing anions (phosphate, silicate) and weak for outer-sphere
2 complexing anions (chloride). The adsorption rate of As(V) and As(III) on PPCI was rapid and
3 most ions were removed within the first 1 h of contact. The kinetic data of PPCI toward both
4 As(V) and As(III) anions fitted better to the PSO model than that to the PFO and Elovich
5 models. The study shows that PPCI is an environmentally friendly material, simple to
6 synthesize and can successfully and efficiently remove the two forms of As from water.

7

8 **Acknowledgement**

9 The first author thanks the University of Technology Sydney for a PhD studentship and
10 the VNU Key Laboratory of Geo-environment and Climate Change Response for assistance in
11 conducting experiments.

12

13 **References**

- 14 Ahmad, I., Farwa, U., Khan, Z.U.H., Imran, M., Khalid, M.S., Zhu, B., Rasool, A., Shah, G.M., Tahir,
15 M. and Ahmed, M. 2022. Biosorption and health risk assessment of arsenic contaminated water
16 through cotton stalk biochar. *Surfaces and Interfaces*. 29, 101806.
- 17 Amen, R., Bashir, H., Bibi, I., Shaheen, S.M., Niazi, N.K., Shahid, M., Hussain, M.M., Antoniadis, V.,
18 Shakoor, M.B., Al-Solaimani, S.G., Wang, H., Bundschuh, J. and Rinklebe, J. 2020. A critical
19 review on arsenic removal from water using biochar-based sorbents: The significance of
20 modification and redox reactions. *Chemical Engineering Journal*. 396, 125195.
- 21 Arcibar-Orozco, J.A., Josue, D.B., Rios-Hurtado, J.C. and Rangel-Mendez, J.R. 2014. Influence of
22 iron content, surface area and charge distribution in the arsenic removal by activated carbons.
23 *Chemical Engineering Journal*. 249, 201-209.
- 24 Aredes, S., Klein, B. and Pawlik, M. 2013. The removal of arsenic from water using natural iron oxide
25 minerals. *Journal of Cleaner Production*. 60, 71-76.
- 26 Baig, S.A., Lou, Z., Hayat, M.T., Fu, R., Liu, Y. and Xu, X. 2016. Characterization of magnetic biochar
27 amended with silicon dioxide prepared at high temperature calcination. *Materials Science*
28 *Poland*. 34(3), 597-604.
- 29 Blanchard, G., Maunaye, M. and Martin, G. 1984. Removal of heavy metals from waters by means of
30 natural zeolites. *Water Research*. 18(12), 1501-1507.
- 31 Chang, Q., Lin, W. and Ying, W.C. 2010. Preparation of iron-impregnated granular activated carbon
32 for arsenic removal from drinking water. *Journal of Hazardous Materials*. 184(1-3), 515-522.
- 33 Chang, Y.Y., Song, K.H. and Yang, J.K. 2008. Removal of As (III) in a column reactor packed with
34 iron-coated sand and manganese-coated sand. *Journal of Hazardous Materials*. 150(3), 565-572.

- 1 Chaudhry, S.A., Zaidi, Z. and Siddiqui, S.I. 2017. Isotherm, kinetic and thermodynamics of arsenic
2 adsorption onto Iron-Zirconium Binary Oxide-Coated Sand (IZBOCS): modelling and process
3 optimization. *Journal of Molecular Liquids*. 229, 230-240.
- 4 Cheng, D., Ngo, H.H., Guo, W., Chang, S.W., Nguyen, D.D., Zhang, X., Varjani, S. and Liu, Y. 2020.
5 Feasibility study on a new pomelo peel derived biochar for tetracycline antibiotics removal in
6 swine wastewater. *Science of The Total Environment*. 720, 137662.
- 7 Choong, T.S., Chuah, T., Robiah, Y., Koay, F.G. and Azni, I. 2007. Arsenic toxicity, health hazards
8 and removal techniques from water: an overview. *Desalination*. 217(1-3), 139-166.
- 9 Chowdhury, S.R. and Yanful, E.K. 2010. Arsenic and chromium removal by mixed magnetite–
10 maghemite nanoparticles and the effect of phosphate on removal. *Journal of Environmental
11 Management*. 91(11), 2238-2247.
- 12 Cope, C.O., Webster, D.S. and Sabatini, D.A. 2014. Arsenate adsorption onto iron oxide amended rice
13 husk char. *Science of The Total Environment*. 488, 554-561.
- 14 Coville, N.J. and Tshavhungwe, A.M. 2010. Mesoporous ethanesilica materials with bimodal and
15 trimodal pore-size distributions synthesised in the presence of cobalt ions. *South African Journal
16 of Science*. 106(7), 1-5.
- 17 Dixit, S. and Hering, J.G. 2003. Comparison of arsenic (V) and arsenic (III) sorption onto iron oxide
18 minerals: implications for arsenic mobility. *Environmental Science Technology*. 37(18), 4182-
19 4189.
- 20 Dong, F.X., Yan, L., Zhou, X.H., Huang, S.T., Liang, J.Y., Zhang, W.X., Guo, Z.W., Guo, P.R., Qian,
21 W. and Kong, L.J. 2021. Simultaneous adsorption of Cr (VI) and phenol by biochar-based iron
22 oxide composites in water: Performance, kinetics and mechanism. *Journal of Hazardous
23 Materials*. 416, 125930.
- 24 Duan, X., Zhang, C., Srinivasakannan, C. and Wang, X. 2017. Waste walnut shell valorization to iron
25 loaded biochar and its application to arsenic removal. *Resource-Efficient Technologies*. 3(1),
26 29-36.
- 27 El-Naggar, N.E.A., Rabei, N.H. and El-Malkey, S.E. 2020. Eco-friendly approach for biosorption of
28 Pb^{2+} and carcinogenic Congo red dye from binary solution onto sustainable *Ulva lactuca*
29 biomass. *Scientific Reports*. 10(1), 1-22.
- 30 Faria, M.C., Rosemberg, R.S., Bomfeti, C.A., Monteiro, D.S., Barbosa, F., Oliveira, L.C., Rodriguez,
31 M., Pereira, M.C. and Rodrigues, J.L. 2014. Arsenic removal from contaminated water by
32 ultrafine δ -FeOOH adsorbents. *Chemical Engineering Journal*. 237, 47-54.
- 33 Foroutan, R., Mohammadi, R., Adeleye, A.S., Farjadfard, S., Esvandi, Z., Arfaeinia, H., Sorial, G.A.,
34 Ramavandi, B. and Sahebi, S. 2019. Efficient arsenic (V) removal from contaminated water
35 using natural clay and clay composite adsorbents. *Environmental Science Pollution Research*.
36 26(29), 29748-29762.
- 37 Freundlich, H. 1907. Über die adsorption in lösungen. *Zeitschrift für Physikalische Chemie*. 57(1),
38 385-470.
- 39 Hao, L., Liu, M., Wang, N. and Li, G. 2018. A critical review on arsenic removal from water using
40 iron-based adsorbents. *RSC Advances*. 8(69), 39545-39560.
- 41 He, R., Peng, Z., Lyu, H., Huang, H., Nan, Q. and Tang, J. 2018. Synthesis and characterization of an
42 iron-impregnated biochar for aqueous arsenic removal. *Science of the Total Environment*. 612,
43 1177-1186.
- 44 Herbel, M. and Fendorf, S. 2006. Biogeochemical processes controlling the speciation and transport of
45 arsenic within iron coated sands. *Chemical Geology*. 228(1-3), 16-32.
- 46 Hongtao, L., Shuxia, L., Hua, Z., Yanling, Q., Daqiang, Y., Jianfu, Z. and Zhiliang, Z. 2018.
47 Comparative study on synchronous adsorption of arsenate and fluoride in aqueous solution onto
48 MgAlFe-LDHs with different intercalating anions. *RSC Advances*. 8(58), 33301-33313.

- 1 Jayarajan, M., Arunachalam, R. and Annadurai, G. 2011. Use of low cost nano-porous materials of
2 pomelo fruit peel wastes in removal of textile dye. *Research Journal of Environmental Sciences*.
3 5(5), 434.
- 4 Jeon, C.S., Baek, K., Park, J.K., Oh, Y.K. and Lee, S.D. 2009. Adsorption characteristics of As (V) on
5 iron-coated zeolite. *Journal of Hazardous Materials*. 163(2-3), 804-808.
- 6 Jiménez-Cedillo, M., Olguín, M., Fall, C. and Colín, A. 2011. Adsorption capacity of iron-or iron-
7 manganese-modified zeolite-rich tuffs for As (III) and As (V) water pollutants. *Applied Clay*
8 *Science*. 54(3-4), 206-216.
- 9 Kalaruban, M., Loganathan, P., Nguyen, T.V., Nur, T., Hasan Johir, M.A., Nguyen, T.H., Trinh, M.V.
10 and Vigneswaran, S. 2019. Iron-impregnated granular activated carbon for arsenic removal:
11 Application to practical column filters. *Journal of Environmental Management*. 239, 235-243.
- 12 Kasiuliene, A., Carabante, I., Bhattacharya, P., Caporale, A.G., Adamo, P. and Kumpiene, J. 2018.
13 Removal of metal (oid) s from contaminated water using iron-coated peat sorbent.
14 *Chemosphere*. 198, 290-296.
- 15 Khatamian, M., Khodakarampoor, N. and Saket-Oskoui, M. 2017. Efficient removal of arsenic using
16 graphene-zeolite based composites. *Journal of Colloid and Interface Science*. 498, 433-441.
- 17 Kim, J., Song, J., Lee, S.M. and Jung, J. 2019. Application of iron-modified biochar for arsenite
18 removal and toxicity reduction. *Journal of Industrial Engineering Chemistry*. 80, 17-22.
- 19 Kim, K.W., Chanpiwat, P., Hanh, H.T., Phan, K. and Sthiannopkao, S. 2011. Arsenic geochemistry of
20 groundwater in Southeast Asia. *Frontiers of Medicine*. 5(4), 420-433.
- 21 Kundu, S. and Gupta, A. 2006. Adsorptive removal of As (III) from aqueous solution using iron oxide
22 coated cement (IOCC): evaluation of kinetic, equilibrium and thermodynamic models.
23 *Separation Purification Technology*. 51(2), 165-172.
- 24 Kuriakose, S., Singh, T.S. and Pant, K.K. 2004. Adsorption of As (III) from aqueous solution onto iron
25 oxide impregnated activated alumina. *Water Quality Research Journal*. 39(3), 258-266.
- 26 Lagergren, S.K. 1898. About the theory of so-called adsorption of soluble substances. *Sven.*
27 *Vetenskapsakad. Handlingar*. 24, 1-39.
- 28 Lakshmiathiraj, P., Narasimhan, B., Prabhakar, S. and Raju, G.B.J.J.o.h.m. 2006. Adsorption of
29 arsenate on synthetic goethite from aqueous solutions. *Journal of Hazardous Materials*. 136(2),
30 281-287.
- 31 Langmuir, I. 1918. The adsorption of gases on plane surfaces of glass, mica and platinum. *Journal of*
32 *the American Chemical society*. 40(9), 1361-1403.
- 33 Lee, H.H., Hirano, Y., Murayama, N., Matsumoto, S. and Shibata, J. 2007. Adsorption properties of
34 activated carbon prepared from waste beer lees by KOH activation and CO₂ activation.
35 *Resources Processing*. 54(1), 19-24.
- 36 Lenoble, V., Laclautre, C., Serpaud, B., Deluchat, V. and Bollinger, J.C. 2004. As (V) retention and
37 As (III) simultaneous oxidation and removal on a MnO₂-loaded polystyrene resin. *Science of*
38 *the Total Environment*. 326(1-3), 197-207.
- 39 Li, J.H, Lv, G.H, Bai, W.B, Liu, Q., Zhang, Y.C. and Song, J.Q. 2016a. Modification and use of biochar
40 from wheat straw (*Triticum aestivum* L.) for nitrate and phosphate removal from water.
41 *Desalination Water Treatment*. 57(10), 4681-4693.
- 42 Li, T., Bai, X., Qi, Y.X., Lun, N. and Bai, Y.J. 2016b. Fe₃O₄ nanoparticles decorated on the biochar
43 derived from pomelo pericarp as excellent anode materials for Li-ion batteries. *Electrochimica*
44 *Acta*. 222, 1562-1568.
- 45 Li, Y., Zhang, F.S. and Xiu, F.R. 2009. Arsenic (V) removal from aqueous system using adsorbent
46 developed from a high iron-containing fly ash. *Science of the Total Environment*. 407(21),
47 5780-5786.

- 1 Li, Z., Jean, J.S., Jiang, W.T., Chang, P.H., Chen, C.J. and Liao, L. 2011. Removal of arsenic from
2 water using Fe-exchanged natural zeolite. *Journal of Hazardous Materials*. 187(1-3), 318-323.
- 3 Liang, Q., Ye, L., Huang, Z.H., Xu, Q., Bai, Y., Kang, F. and Yang, Q.H. 2014. A honeycomb-like
4 porous carbon derived from pomelo peel for use in high-performance supercapacitors.
5 *Nanoscale*. 6(22), 13831-13837.
- 6 Lim, L.B., Priyantha, N., Lu, Y. and Zaidi, N. 2019. Adsorption of heavy metal lead using *Citrus*
7 *grandis* (Pomelo) leaves as low-cost adsorbent. *Desalination and Water Treatment*. 166, 44-52.
- 8 Lin, L., Qiu, W., Wang, D., Huang, Q., Song, Z. and Chau, H.W. 2017. Arsenic removal in aqueous
9 solution by a novel Fe-Mn modified biochar composite: characterization and mechanism.
10 *Ecotoxicology Environmental Safety*. 144, 514-521.
- 11 Litter, M.I., Ingallinella, A.M., Olmos, V., Savio, M., Difeo, G., Botto, L., Torres, E.M.F., Taylor, S.,
12 Frangie, S. and Herkovits, J. 2019. Arsenic in Argentina: technologies for arsenic removal
13 from groundwater sources, investment costs and waste management practices. *Science of the*
14 *Total Environment*. 690, 778-789.
- 15 Liu, D.X., Mu, J., Yao, Q., Bai, Y., Qian, F., Liang, F., Shi, F.N. and Gao, J. 2019. Design of iron-ion-
16 doped pomelo peel biochar composites towards removal of organic pollutants. *SN Applied*
17 *Sciences*. 1(2), 184.
- 18 Loganathan, P., Vigneswaran, S., Kandasamy, J. and Bolan, N.S. 2014. Removal and recovery of
19 phosphate from water using sorption. *Critical Reviews in Environmental Science and*
20 *Technology*. 44(8), 847-907.
- 21 Matis, K., Zouboulis, A., Malamas, F., Afonso, M.R. and Hudson, M. 1997. Flotation removal of As
22 (V) onto goethite. *Environmental Pollution*. 97(3), 239-245.
- 23 McLintock, I.S. 1967. The Elovich Equation in Chemisorption Kinetics. *Nature*. 216, 1204.
- 24 Mohan, D. and Pittman Jr, C.U. 2007. Arsenic removal from water/wastewater using adsorbents—a
25 critical review. *Journal of Hazardous Materials*. 142(1-2), 1-53.
- 26 Mondal, P., Balomajumder, C. and Mohanty, B. 2007. A laboratory study for the treatment of arsenic,
27 iron, and manganese bearing ground water using Fe³⁺ impregnated activated carbon: effects of
28 shaking time, pH and temperature. *Journal of Hazardous Materials*. 144(1-2), 420-426.
- 29 Nguyen, T.H., Tran, H.N., Nguyen, T.V., Vigneswaran, S., Nguyen, T.D., Nguyen, T.H.H., Mai, T.N.
30 and Chao, H.P. 2021. Single-step removal of arsenite ions from water through oxidation-
31 coupled adsorption using Mn/Mg/Fe layered double hydroxide as catalyst and adsorbent.
32 *Chemosphere*. 133370.
- 33 Nguyen, T.H., Tran, H.N., Vu, H.A., Trinh, M.V., Nguyen, T.V., Loganathan, P., Vigneswaran, S.,
34 Nguyen, T.M., Trinh, V.T., Vu, D.L. and Nguyen, T.H.H. 2020a. Laterite as a low-cost
35 adsorbent in a sustainable decentralized filtration system to remove arsenic from groundwater
36 in Vietnam. *Science of The Total Environment*. 699, 134267.
- 37 Nguyen, T.T.Q., Loganathan, P., Nguyen, T.V. and Vigneswaran, S. 2020b. Removing arsenate from
38 water using modified manganese oxide ore: Column adsorption and waste management. *Journal*
39 *of Environmental Chemical Engineering*. 8(6), 104491.
- 40 Nguyen, T.T.Q., Loganathan, P., Nguyen, T.V., Vigneswaran, S. and Ngo, H.H. 2020c. Iron and
41 zirconium modified luffa fibre as an effective bioadsorbent to remove arsenic from drinking
42 water. *Chemosphere*. 258, 127370.
- 43 Nguyen, T.V., Nguyen, T.V.T., Pham, T.L., Vigneswaran, S., Ngo, H.H., Kandasamy, J., Nguyen, H.K.
44 and Nguyen, D.T. 2009. Adsorption and removal of arsenic from water by iron ore mining
45 waste. *Water Science and Technology*. 60(9), 2301-2308.
- 46 Nguyen, V.H., Van, H.T., Nguyen, V.Q., Dam, X.V., Hoang, L. and Ha, L. 2020d. Magnetic Fe₃O₄
47 nanoparticle biochar derived from pomelo peel for reactive red 21 adsorption from aqueous
48 solution. *Journal of Chemistry*. 2020(2),1-14.

- 1 Nham, N.T., Al Tahtamouni, T., Nguyen, T.D., Huong, P.T., Jitae, K., Viet, N.M., Van Noi, N., Phuong,
2 N.M. and Anh, N.T.H. 2019. Synthesis of iron modified rice straw biochar toward arsenic from
3 groundwater. *Materials Research Express*. 6(11), 115528.
- 4 Oliveira, L.C.A., Pereira, E., Guimaraes, I.R., Vallone, A., Pereira, M., Mesquita, J.P. and Sapag, K.
5 2009. Preparation of activated carbons from coffee husks utilizing FeCl₃ and ZnCl₂ as activating
6 agents. *Journal of Hazardous Materials*. 165(1), 87-94.
- 7 Omorogie, M.O., Babalola, J.O., Unuabonah, E.I., Song, W. and Gong, J.R. 2016. Efficient chromium
8 abstraction from aqueous solution using a low-cost biosorbent: *Nauclea diderrichii* seed biomass
9 waste. *Journal of Saudi Chemical Society*. 20(1), 49-57.
- 10 Pehlivan, E., Tran, T., Ouédraogo, W., Schmidt, C., Zachmann, D. and Bahadir, M. 2013. Removal of
11 As (V) from aqueous solutions by iron coated rice husk. *Fuel Processing Technology*. 106, 511-
12 517.
- 13 Pereira, R.C., Anizelli, P.R., Di Mauro, E., Valezi, D.F., Da Costa, A.C.S., Zaia, C.T.B. and Zaia, D.A.
14 2019. The effect of pH and ionic strength on the adsorption of glyphosate onto ferrihydrite.
15 *Geochemical Transactions*. 20(1), 1-14.
- 16 Pierce, M.L. and Moore, C.B. 1982. Adsorption of arsenite and arsenate on amorphous iron hydroxide.
17 *Water Research*. 16(7), 1247-1253.
- 18 Pintor, A.M., Vieira, B.R., Santos, S.C., Boaventura, R.A. and Botelho, C.M. 2018. Arsenate and
19 arsenite adsorption onto iron-coated cork granulates. *Science of the Total Environment*. 642,
20 1075-1089.
- 21 Pizarro, C., Escudey, M., Caroca, E., Pavez, C. and Zúñiga, G.E. 2021. Evaluation of zeolite,
22 nanomagnetite, and nanomagnetite-zeolite composite materials as arsenic (V) adsorbents in
23 hydroponic tomato cultures. *Science of the Total Environment*. 751, 141623.
- 24 Redlich, O. and Peterson, D.L. 1959. A useful adsorption isotherm. *Journal of Physical Chemistry*.
25 63(6), 1024-1024.
- 26 Saikaew, W., Kaewsarn, P. and Saikaew, W. 2009. Pomelo peel: agricultural waste for biosorption of
27 cadmium ions from aqueous solutions. *World Academy of Science, Engineering and
28 Technology*. 56, 287-291.
- 29 Samsuri, A.W., Sadegh-Zadeh, F. and Seh-Bardan, B.J. 2013. Adsorption of As(III) and As(V) by Fe
30 coated biochars and biochars produced from empty fruit bunch and rice husk. *Journal of
31 Environmental Chemical Engineering*. 1(4), 981-988.
- 32 Smedley, P.L. and Kinniburgh, D.G. 2002. A review of the source, behaviour and distribution of arsenic
33 in natural waters. *Applied Geochemistry*. 17(5), 517-568.
- 34 Smith, M., Cross, K., Paden, M. and Laban, P. 2016. Spring–Managing groundwater sustainably.
35 IUCN, Gland, Switzerland.
- 36 Tasaso, P. 2014. Adsorption of copper using pomelo peel and depectinated pomelo peel. *Journal of
37 Clean Energy Technologies*. 2(2), 154-157.
- 38 Thommes, M., Kaneko, K., Neimark, A.V., Olivier, J.P., Rodriguez-Reinoso, F., Rouquerol, J. and Sing,
39 K.S. 2015. Physisorption of gases, with special reference to the evaluation of surface area and
40 pore size distribution (IUPAC Technical Report). *Pure Applied Chemistry*. 87(9-10), 1051-
41 1069.
- 42 Tian, Y., Wu, M., Lin, X., Huang, P. and Huang, Y. 2011. Synthesis of magnetic wheat straw for
43 arsenic adsorption. *Journal of Hazardous Materials*. 193, 10-16.
- 44 Tocmo, R., Pena-Fronteras, J., Calumba, K.F., Mendoza, M. and Johnson, J.J. 2020. Valorization of
45 pomelo (*Citrus grandis* Osbeck) peel: A review of current utilization, phytochemistry,
46 bioactivities, and mechanisms of action. *Comprehensive Reviews in Food Science and Food
47 Safety*. 19(4), 1969-2012.
- 48 Tomul, F., Arslan, Y., Kabak, B., Trak, D., Kendüzler, E., Lima, E.C. and Tran, H.N. 2020. Peanut
49 shells-derived biochars prepared from different carbonization processes: Comparison of

- 1 characterization and mechanism of naproxen adsorption in water. *Science of the Total*
2 *Environment*. 726, 137828.
- 3 Tran, H.N., You, S.J. and Chao, H.P. 2016. Effect of pyrolysis temperatures and times on the adsorption
4 of cadmium onto orange peel derived biochar. *Waste Management & Research*. 34(2), 129-138.
- 5 Tseng, C.H., Tai, T.Y., Chong, C.K., Tseng, C.P., Lai, M.S., Lin, B.J., Chiou, H.Y., Hsueh, Y.M., Hsu,
6 K.H. and Chen, C.J. 2000. Long-term arsenic exposure and incidence of non-insulin-dependent
7 diabetes mellitus: a cohort study in arseniasis-hyperendemic villages in Taiwan. *Environmental*
8 *Health Perspectives*. 108(9), 847-851.
- 9 Verma, L. and Singh, J. 2019. Synthesis of novel biochar from waste plant litter biomass for the
10 removal of arsenic (III and V) from aqueous solution: A mechanism characterization, kinetics
11 and thermodynamics. *Journal of Environmental Management*. 248, 109235.
- 12 Vieira, B.R., Pintor, A.M., Boaventura, R.A., Botelho, C.M. and Santos, S.C. 2017. Arsenic removal
13 from water using iron-coated seaweeds. *Journal of Environmental Management*. 192, 224-233.
- 14 Vithanage, M., Herath, I., Joseph, S., Bundschuh, J., Bolan, N., Ok, Y.S., Kirkham, M.B. and Rinklebe,
15 J. 2017. Interaction of arsenic with biochar in soil and water: A critical review. *Carbon*. 113,
16 219-230.
- 17 Water, S. and Organization, W.H. 2004. Guidelines for drinking-water quality. Vol. 1,
18 Recommendations.
- 19 Weerasundara, L., Ok, Y.S. and Bundschuh, J. 2021. Selective removal of arsenic in water: A critical
20 review. *Environmental Pollution*. 268, 115668.
- 21 Wu, Y., Cha, L., Fan, Y., Fang, P., Ming, Z. and Sha, H. 2017. Activated biochar prepared by pomelo
22 peel using H_3PO_4 for the adsorption of hexavalent chromium: performance and mechanism.
23 *Water, Air, Soil Pollution*. 228(10), 1-13.
- 24 Yang, J.S., Kim, Y.S., Park, S.M. and Baek, K. 2014. Removal of As (III) and As (V) using iron-rich
25 sludge produced from coal mine drainage treatment plant. *Environmental Science and Pollution*
26 *Research*. 21(18), 10878-10889.
- 27 Yao, S., Liu, Z. and Shi, Z. 2014. Arsenic removal from aqueous solutions by adsorption onto iron
28 oxide/activated carbon magnetic composite. *Journal of Environmental Health Science*
29 *Engineering*. 12(1), 1-8.
- 30 Yee, J.J., Arida, C.V.J., Futralan, C.M., De Luna, M.D.G. and Wan, M.W. 2019. Treatment of
31 contaminated groundwater via arsenate removal using chitosan-coated bentonite. *Molecules*.
32 24(13), 2464.
- 33 Zhang, B., Wu, Y. and Cha, L. 2019. Removal of methyl orange dye using activated biochar derived
34 from pomelo peel wastes: performance, isotherm, and kinetic studies. *Journal of Dispersion*
35 *Science Technology*. 41, 1-12.
- 36 Zhang, F.S. and Itoh, H. 2005. Iron oxide-loaded slag for arsenic removal from aqueous system.
37 *Chemosphere*. 60(3), 319-325.
- 38 Zhang, M., Gao, B., Varnoosfaderani, S., Hebard, A., Yao, Y. and Inyang, M. 2013. Preparation and
39 characterization of a novel magnetic biochar for arsenic removal. *Bioresource Technology*. 130,
40 457-462.
- 41